AD-A179 779 STUDY OF SUBMICRON PARTICLE SIZE DISTRIBUTION BY LASER 1/1
DOPPLER MEASUREMEN..(U) AERODYNE RESEARCH INC BILLERICA
MA W K CHENG ET AL. 30 JAN 87 ARI-RR-563
UNCLASSIFIED AFOSR-TR-87-0566 F49620-83-C-0154 F/G 20/6 NL

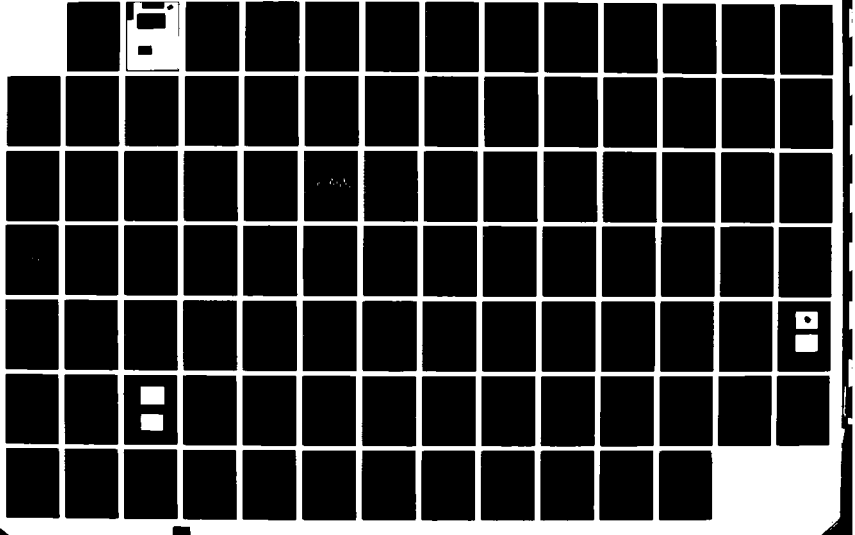

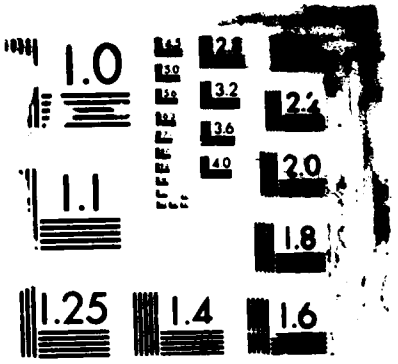
1.0
1.1
1.25
1.4
1.6
1.8
2.0
2.2
2.8
3.2
3.6
4.0

STUDY OF SUBMICRON PARTICLE SIZE DISTRIBUTION BY LASER DOPPLER MEASUREMENT OF BROWNIAN MOTION

ARI-RR-563

STUDY OF SUBMICRON PARTICLE SIZE DISTRIBUTION BY LASER DOPPLER MEASUREMENT OF BROWNIAN MOTION

Prepared by

Wai K. Cheng, Keith E. McCurdy, Sarah Kostic, Alan Stanton,
and Joda Wormhoudt
Aerodyne Research, Inc.
45 Manning Road
Billerica, MA 01821

Prepared for

Air Force Office of Scientific Research
Building 410
Bolling AFB, DC 20332

Final Technical Report

Contract No. F49620--83-C-0154

March 1987

SECURITY CLASSIFICATION OF THIS PAGE

REPORT DOCUMENTATION PAGE

1a. REPORT SECURITY CLASSIFICATION: Unclassified	1b. RESTRICTIVE MARKINGS: None
2a. SECURITY CLASSIFICATION AUTHORITY	3. DISTRIBUTION / AVAILABILITY OF REPORT: Distribution unlimited; approved for public release
2b. DECLASSIFICATION / DOWNGRADING SCHEDULE	
4. PERFORMING ORGANIZATION REPORT NUMBER(S): ARI-RR-563	5. MONITORING ORGANIZATION REPORT NUMBER(S): AFOSR-TR- 87-0566
6a. NAME OF PERFORMING ORGANIZATION: Aerodyne Research, Inc. / 6b. OFFICE SYMBOL (If applicable)	7a. NAME OF MONITORING ORGANIZATION: Air Force Office of Scientific Research
6c. ADDRESS (City, State, and ZIP Code): 45 Manning Road, Billerica, MA 01821	7b. ADDRESS (City, State, and ZIP Code): NC 410, Bolling AFB DC 20332-6448
8a. NAME OF FUNDING / SPONSORING ORGANIZATION: Air Force Office of Sci. Res. / 8b. OFFICE SYMBOL (If applicable): AFOSR/NA	9. PROCUREMENT INSTRUMENT IDENTIFICATION NUMBER: F49620-83-C-0154
8c. ADDRESS (City, State, and ZIP Code): BIC 410, Bolling AFB DC 20332-6448	10. SOURCE OF FUNDING NUMBERS: PROGRAM ELEMENT NO. 61102F; PROJECT NO 2308; TASK NO. A3; WORK UNIT ACCESSION NO.

11. TITLE (Include Security Classification)
Study of Submicron Particle Size Distribution by Laser Doppler Measurement of Brownian Motion

12. PERSONAL AUTHOR(S)
Wai K. Cheng, Keith E. McCurdy, Sarah Kostic, and Joda Wormhoudt

13a. TYPE OF REPORT	13b. TIME COVERED	14. DATE OF REPORT (Year, Month, Day)	15. PAGE COUNT
Final	FROM 9/1/83 TO 9/30/86	January 30, 1987	83

16. SUPPLEMENTARY NOTATION

17. COSATI CODES			18. SUBJECT TERMS (Continue on reverse if necessary and identify by block number)
FIELD	GROUP	SUB-GROUP	Submicron Particles, Brownian Motion, Size Distributions
21	02		
21	05		

19. ABSTRACT (Continue on reverse if necessary and identify by block number)

A theoretical and experimental study on the feasibility of determining the size of a single submicron particle by observing its Brownian motion characteristics has been carried out. The method is based on measurement of the particle motion interferometrically using the light scattered from a pair of intersecting laser beams. The particle is assumed to be in thermal equilibrium with a fluid medium. Due to the viscous damping of the fluid, the motion of the particle exhibits relaxation behavior. The relaxation time may be obtained from the interference signal. Knowing the temperature and the viscosity of the fluid, the mass, hence the size of the particle may be determined from the relaxation time. Monte Carlo simulation of the Brownian motion detector response has shown that the relaxation time may be obtained from the statistics of the time between extrema of the signal. A proof-of-concept experiment was conducted using latex spheres of known sizes as test particles. The signal to noise ratio of the experimental setup, however, was not adequate for determining the size of the particles.

20. DISTRIBUTION / AVAILABILITY OF ABSTRACT	21. ABSTRACT SECURITY CLASSIFICATION
☐ UNCLASSIFIED/UNLIMITED ☒ SAME AS RPT. ☐ DTIC USERS	Unclassified
22a. NAME OF RESPONSIBLE INDIVIDUAL: Julian M. Tishkoff	22b. TELEPHONE (Include Area Code): (202) 767-4935 / 22c. OFFICE SYMBOL: AFOSR/NA

DD FORM 1473, 84 MAR — 83 APR edition may be used until exhausted. All other editions are obsolete.

SECURITY CLASSIFICATION OF THIS PAGE

TABLE OF CONTENTS

LIST OF ILLUSTRATIONS

List of Illustrations (Continued)

List of Illustrations (Continued)

ABSTRACT

A theoretical and experimental study on the feasibility of determining the size of a single submicron particle by observing its Brownian motion characteristics has been carried out. The method is based on measurement of the particle motion interferometrically using the light scattered from a pair of intersecting laser beams. The particle is assumed to be in thermal equilibrium with a fluid medium. Due to the viscous damping of the fluid, the motion of the particle exhibits relaxation behavior. The relaxation time may be obtained from the interference signal. Knowing the temperature and the viscosity of the fluid, the mass, hence the size of the particle may be determined from the relaxation time. Monte Carlo simulation of the Brownian motion detector response has shown that that the relaxation time may be obtained from the statistics of the time between extrema of the signal. A proof-of-concept experiment was conducted using latex spheres of known sizes as test particles. The signal to noise ratio of the experimental setup, however, was not adequate for determining the size of the particles.

1. INTRODUCTION

1.1 Overview

Measurement of particle size in the submicron (0.01 - 0.1 μm) range has many important scientific applications. For example, in the study of soot emission in combustors and burners, the soot formation and oxidation rates can be inferred from the soot particle size evolution. The combustion of coal particles and the formation of fly ash can be studied in a similar manner. Submicron particles are also important in corrosion of boiler surfaces and heat exchangers in electric power plants or chemical processing plants and in erosion of turbine blades in advanced combined cycle processors. Other areas where an understanding of the role of submicron particles is important include the nucleation and condensation processes leading to acid rain, and soot formation and enrichment of polycyclic aromatic hydrocarbons in internal combustion engines. Measurement of submicron particles is basic to an understanding of all of these processes.

In this report, we describe an attempt to develop a technique for accurate, in-situ determination of submicron particle size distributions based on a Laser Doppler measurement of the Brownian motion of the particles. The objective was: to review the scientific basis of the technique, to conduct a proof-of-concept feasibility experiment, to determine through the experiment the practical difficulties of the technique, and to identify the solutions needed to overcome these difficulties.

1.2 Review of Particle Sizing Techniques

In general, particle measurement in the submicron size range can be categorized as either probe sampling techniques[1.1-1.4] or in situ optical techniques.[1.5-1.13] In the sampling probe approach, a vacuum system of varying degree of complexity is used to draw the particle laden stream through

grids or filter paper. The deposited particles are then analyzed by electron microscopy[1.2, 1.3] or optical reflectivity and transmissivity measurements.[1.4] The difficulty in these direct sampling methods is that the surface deposition of the particles influence the particle size distribution in an unknown way. The physical presence of a sampling probe may also interfere with the phenomena under study. This interference is especially severe when high spatial resolution is required.

In situ optical techniques have an advantage over probe sampling because the flow is not disturbed. Optical techniques may be classified as a single particle counting or a volume averaged measurement. In single particle counting, the measurement system examines only one particle at a time and records the particle size. The particle size distribution is obtained by tabulating the sizes of many particles. In the volume averaged method, the measured signals are a convolution of the optical properties of the individual particles and the particle distribution. Therefore, various assumptions have to be made to obtain the size distribution from the measured signals.

The most well developed optical techniques are based on an analysis of the amplitude of the scattered light from the particles. Measurements with various optical configurations have been reported.[1.5-1.13] For example, measurements and analyses were performed with multicolor systems, with light of various polarizations, and on the angular distribution of the scattered light. The interpretation of these measurements is usually based on Mie theory.[1.14, 1.15] A comprehensive review of these measurements is given in Ref. [1.16].

The major disadvantage of the light scattering technique is that the scattered amplitude is sensitive to the optical properties of the particles, which are in general not well known. In general, researchers have interpreted the experimental results based on Mie theory and a refractive index for the particles which is based on bulk measurements.[1.4, 1.17] The validity of using the refractive index of the bulk material is open to question.

Therefore, there is a need to develop an optical particle size measurement scheme which is independent of the optical properties of the particle.

For completeness, we mention other miscellaneous optical sizing schemes. These schemes include the opto-acoustic cell[1.18, 1.19] which is a volume averaged measurement and is dependent on the particle light absorption properties, and the holographic technique,[1.20] which is difficult to apply to particles of size smaller than the wavelength of the illumination.

In this report, we have studied submicron particle sizing in a gas stream by measuring the Doppler shift of the scattered light from the particles in Brownian motion. Since the scheme is a frequency measurement, the result should be independent of the optical properties of the particle. The measured signal is a function of the gas viscosity, which depends on the temperature that can be readily determined independently, and the particle mass, which can be related to the particle size.

This concept of particle size determination is not new.[1.21-1.24] Nevertheless, previous measurements based on this concept have all been interpreted in terms of spectral broadening of the scattered radiation due to the Brownian motion of a large number of particles. Therefore, these measurements were volume averaged. Our approach, however, is to operate in a single particle counting mode in which the individual particle size is inferred from the Brownian motion of a single particle.

1.3 Organization of the Report

The remaining chapters of this report are organized as follows. In Chapter 2, the basic physics of Brownian motion is reviewed. In particular, we have highlighted the statistical nature of the motion, which precludes the measurement of particle velocities by the traditional laser Doppler technique. In Chapter 3, a method for interpreting the information contained in the Doppler signal of the scattered light and a demonstration of the concept in a Monte Carlo computer simulation of the signal are

discussed. The theoretical basis for the method is described in Chapter 4. In Chapter 5, the signal to noise required for adequate signal detection is estimated and the experimental set up for the proof-of-concept demonstration is described. The analysis of the signal obtained in this experiment is then presented. It was concluded that the signal is dominated by shot noise and the Brownian motion information cannot be recovered from the signal. In Chapter 6, we examine some of the physical limitations on the improvement of S/N by increasing the beam intensity. The summary and conclusions of this project are presented in Chapter 7.

1.4 References for Chapter 1

1.1 Erickson, W.D., Williams, G.C., Hottel, H.C., "Light Scattering Measurements on Soot in a Benzene-Air Flame," Combust. and Flame, 8, 127 (1964).

1.2 Shaffernocker, W.M., Stanforth, M., "Smoke Measurement Techniques," SAE paper 680346 (1968).

1.3 Wersborg, B.L., Howard, J.B., Williams, G.C., "Physical Mechanisms in Carbon Formation in Flames," 14th Int. Symp. on Combustion (1973).

1.4 Dalzell, W.H., Sarofim, A.F., "Optical Constants of Soot and Their Application to Heat-Flux Calculations," Transactions of ASME, J. Heat Transf., 91, 100 (1969).

1.5 Kunugi, M., Jinno, H., "Determination of Size and Concentration of Soot Particles in Diffusion Flames by a Light Scattering Technique," 11th Symposium on Combustion, 257 (1967).

1.6 Hodkinson, J.R., "Particle Sizing by Means of the Forward Scattering Lobe," Appl. Optics, 5, 839 (1966).

1.7 Muly, E.C., Frock, H.N., "Industrial Particle Size Measurement Using Light Scattering," Optical Engineering, 19, 861 (1980).

1.8 Chigier, N.A., "Measurement in Multiphase Reacting Flows - A Review," AIAA paper 79-0082 (1979).

1.9 Jones, A.R., "A Review of Droplet Size Measurement - The Application of Techniques to Dense Fuel Sprays," Prog. Energy Combust. Sci., 3, 225 (1977).

1.10 Bonczyk, P.A., "Measurements of Particle Size by in situ Laser-Optical Methods: A Critical Evaluation Applied to Fuel-Pyrolyzed Carbon," Combust. and Flame, 35, 191 (1979).

1.11 Hirleman, E.D., "Laser Based Single Particle Counters for in situ Particle Diagnostics," Optical Engineering, 19, 854 (1980).

1.12 Holve, D., Self, S.A., "Optical Particle Sizing for in situ Measurements, Part I and II," Appl. Optics, 18, 1632 (1979).

1.13 Phillips, D.T., Wyatt, P.J., "Single-Particle Light Scattering Measurement: Photochemical Aerosols and Atmospheric Particulates," Appl. Optics, 11, 2082 (1972).

1.14 van de Hulst, H.C., Light Scattering by Small Particles, Wiley, New York (1957).

1.15 Kerker, M., The Scattering of Light, Academic Press, New York (1969).

1.16 D'Alessio, A., "Laser Light Scattering and Fluorescence Diagnostics of Rich Flames Produced by Gaseous and Liquid Fuels," General Motors Symposium on "Particulate Carbon: Formation During Combustion," General Motors Research Lab., Warren, Michigan (1980).

1.17 Senftlehen, H., Benedict, E., "Uber die optisches Konstanten und die Strahlungsgesetze des Kohle," Ann. Der Phys. 54, 65 (1918).

1.18 Foxvog, F.R., Roessler, D.M., "Optoacoustic Measurements of Diesel Particulate Emissions," General Motors Research Publication GMR-2987 (1979).

1.19 Bruce, C.W., Pinnick, R.G., "In Situ Measurement of Aerosol Absorption With a Resonant CW Laser Spectrophone," Appl. Optics, 16, 1762 (1977).

1.20 Trolinger, J.P., Field, D., "Particle Field Diagnostics by Holography," AIAA Paper 80-0018 (1980).

1.21 Penner, S.S. Chang, P., "On the Determination of Log-Normal Particle-Size Distribution Using Half Widths and Detectabilities of Scattered Laser Power Spectra," J. Quant. Spect. Rad. Transfer, 20, 447 (1978).

1.22 Russel, W.B., "Brownian Motion of Small Particles Suspended in Liquid," Annual Review of Fluid Mechanics, 13, 425 (1981).

1.23 McDonnell, M.E., Jamieson, A.M., "Quasielastic Light Scattering Measurement of Diffusion Coefficients in Polystyrene Solutions," J. Macromol. Sci., 17 (1977).

1.24 Chang, P.H.P., and Penner, S.S., "Particle-Size Measurements in Flames Using Light Scattering; Comparison With Diffusion-Broadening Spectroscopy," J. Quant. Spectrosc. Radiat. Transfer, 25, 97 (1981).

2. BASIC PHYSICS OF BROWNIAN MOTION

In this chapter, the basic physics of Brownian motion is described. The nature of the motion is such that within the time that the particle traverses a fringe pair in a laser Doppler velocimeter system, its velocity may have changed drastically. Therefore such a system does not yield meaningful velocity measurements. The proper interpretation of the information contained in the Doppler signal will be discussed in Chapter 3.

2.1 The Nature of Brownian Motion

When a small particle is immersed in a fluid medium, it exhibits an irregular motion as a result of the bombardment of the fluid molecules. It should be noted that the momentum transfer to the particle in each collision is extremely small, but the collision frequency is extremely high ($\sim 10^{14}$/s). The motion of the particle is the aggregate effect of a large number of collisions.

A schematic representation of the time dependent motion of a 0.1 μm particle is shown in Figure 2.1 in order to indicate the time scales characteristic of the motion. In this figure, random changes in particle velocity, of order 10^{-5} m$\cdot$s^{-1}, occur in characteristic times of 10^{-14} seconds due to collisions with gas molecules. This time scale is much faster than can be resolved by practical instruments. Therefore, only an aggregate velocity is observable. This aggregate velocity obeys a Maxwellian velocity distribution. The characteristic time for the Maxwellian distribution to develop is the "relaxation time" t_{relax} ($\approx 10^{-7}$ s in Figure 2.1), which is a function of particle size and fluid properties. Clearly if one wants to obtain any information on the Brownian motion of an individual particle, one must sample the time history of particle motion in an interval short compared

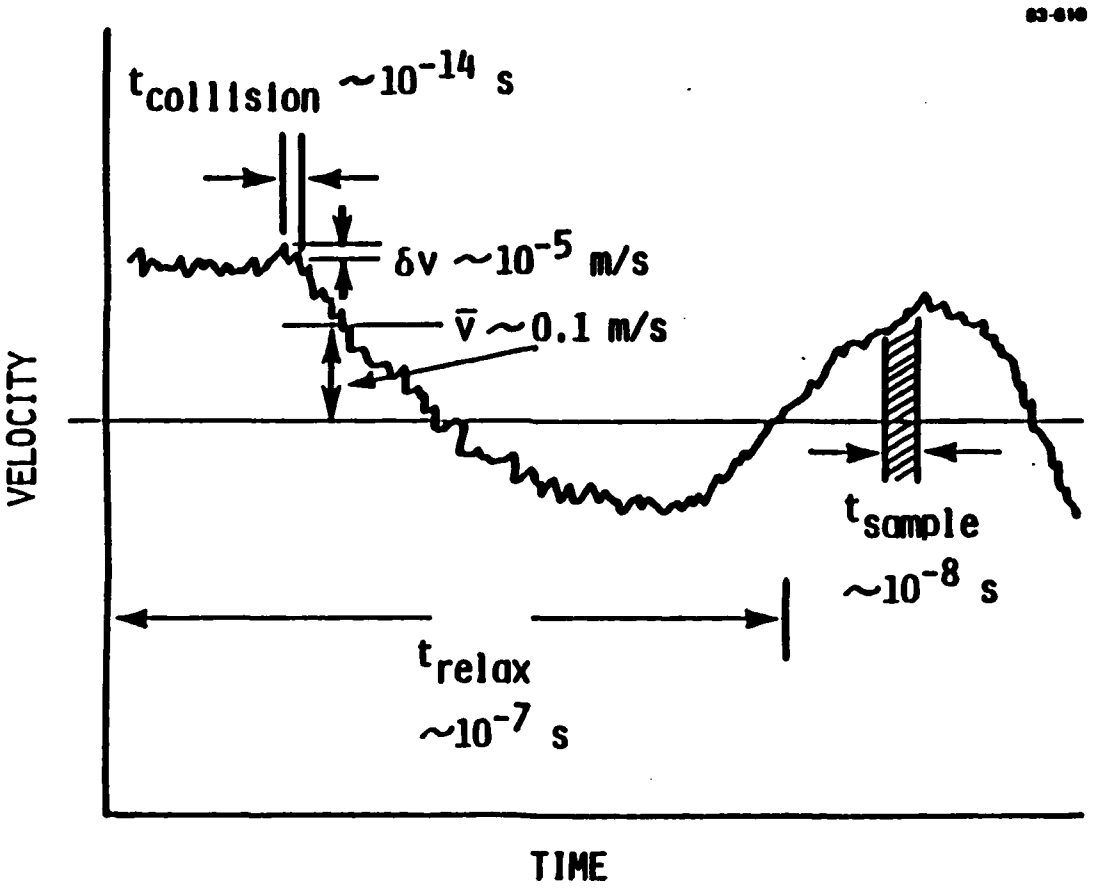

Figure 2.1. Time Dependent Motion of a 0.1 μm Diameter Particle in Air at 300 K and Atmospheric Pressure.

to the relaxation time, or the effects will be averaged out. Conversely, one cannot monitor the instantaneous Brownian velocity of the particle, because electronics and signal-to-noise limitations constrain realizable sampling intervals to be much longer than the 10^{-14} s characteristic collision time. The measurement strategy, then, is to sample with an interval on the order of 10^{-8} s, which is fast compared to the relaxation time. The type of signal measured with this kind of time resolution will be a superposition of many random events, but the time dependence of this signal should exhibit statistical properties representative of the Brownian motion of a particle of a particular size.

The statistical analysis of the Brownian motion of a particle in thermal equilibrium with a fluid medium is described by the Langevin equation:[2.1]

$$\frac{d\underline{u}}{dt} = \beta\underline{u} + \underline{A}(t) \tag{2.1}$$

where $\underline{u}$ is the velocity and β is the damping coefficient. The random excitation $\underline{A}(t)$ has the property that the solution of Eq. (1), which is

$$\underline{u} - \underline{u}_o e^{-\beta t} = e^{-\beta t} \int_o^t e^{\beta\xi}\, \underline{A}(\xi)\, d\xi \tag{2.2}$$

has the Maxwellian velocity distribution in the limit of large t. The time scale for approaching this limit is

$$\tau_{relax} = 1/\beta \quad . \tag{2.3}$$

In continuum flow ($\lambda_{mfp} << d$), for a spherical particle of diameter d and mass m, β is given by

$$\beta = 3\pi\mu\, d/m \quad , \tag{2.4}$$

where μ is the viscosity of the fluid medium. For the free flow limit ($\lambda_{mfp} >> d$), the value of β is given by the Epstein formula,

$$\beta = \frac{\pi d^2}{m} \rho_{air} \frac{\bar{c}}{3} \left(1 + \frac{\pi\alpha}{8}\right) \tag{2.5}$$

where $\bar{c}$ is the mean thermal speed of the fluid molecules and α is the accommodation coefficient. A value of $\alpha = 0.5$ was used in the simulation to be described in Chapter 3. Values for the relaxation time are shown in Figure 2.2.

As an example, we consider a particle of 0.2 μm diameter with a specific gravity of 2. For air at 300 K and at 1 atmosphere pressure, the relaxation time is $\tau_{relax} = 150$ ns. To obtain information about the velocity distribution, the sampling time should be less than τ_{relax}. A sampling time Δt of the order of 10 ns was used in the simulation to be described in Chapter 3. Furthermore, a time between samples of 10 ns was assumed.

The time scale for the fluctuating excitation A(t) is of the order of the collision time τ_c between the fluid molecules and the particle, which is $\sim 10^{-14}$ s. During each collision, the particle changes its velocity by

$$\frac{\sqrt{8kT\tilde{m}}}{m} \tag{2.6}$$

where $\tilde{m}$ is the mass of a fluid molecule. The value for δV is $\sim 10^{-5}$ m$\cdot$s^{-1}.

Since the sampling time Δt is large compared to the collision time τ_c, the velocity sampled is the average over Δt of the time dependent velocity given by Eq. (2.2). The requirement that the velocity distribution has the asymptotic limit of a Maxwellian distribution requires the sampled velocity $\underline{w}_n$ at $n\Delta t$ to have a probability distribution of,[2.1]

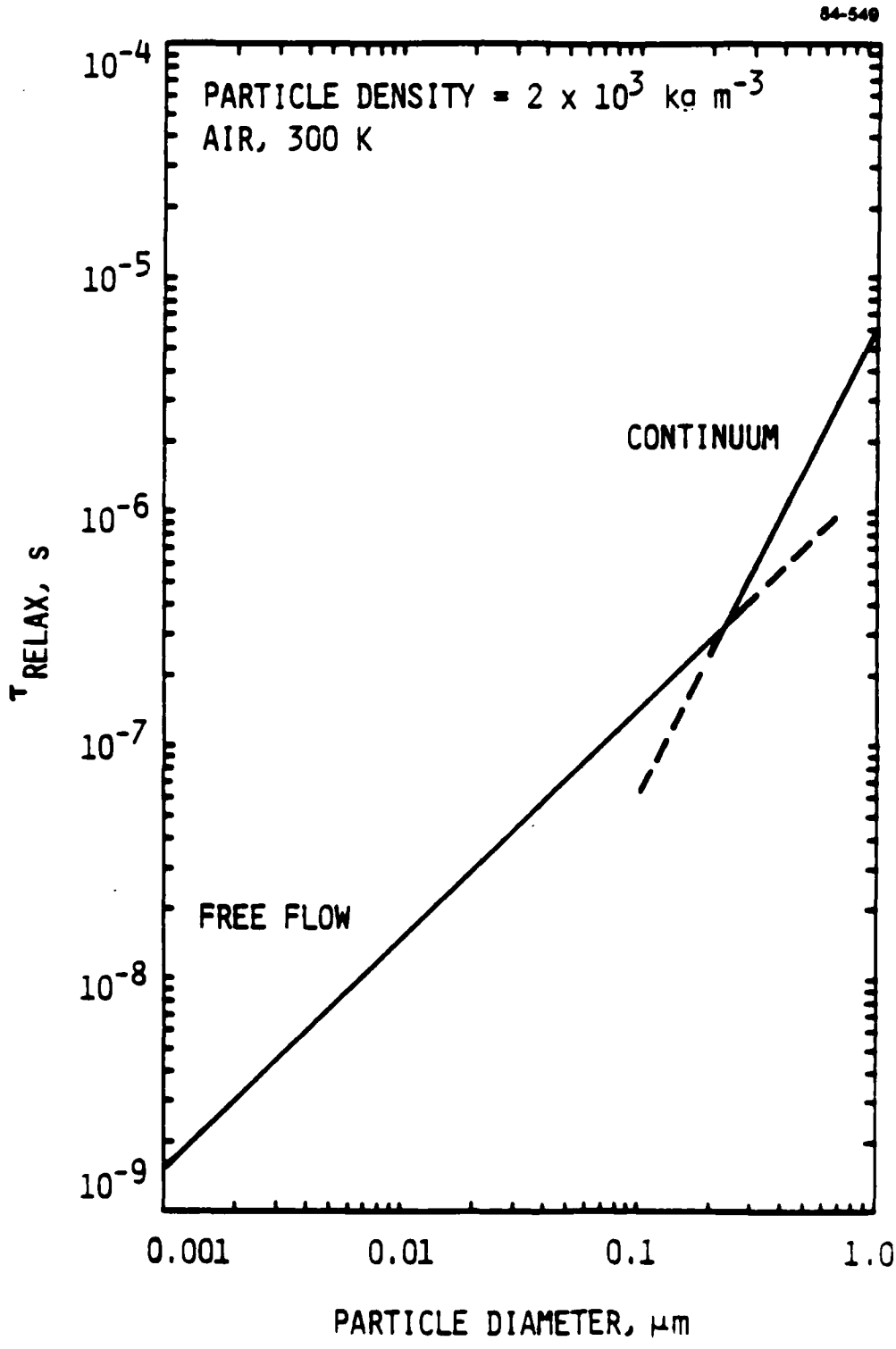

Figure 2.2. Characteristic Relaxation Time for Particles in Brownian Motion.

$$p(\underline{w}_n,\Delta t\ ;\ \underline{w}_{n-1}) = \left[\frac{m}{2\pi kT\ (1-e^{-2\beta\Delta t})}\right]^{3/2} \exp\left[\frac{-m\ \left|\ \underline{w}_n - \underline{w}_{n-1}e^{-\beta\Delta t}\ \right|^2}{2kT\ (1-e^{-2\beta\Delta t})}\right] . \tag{2.7}$$

Therefore, if $\underline{w}_n = (u_n,v_n,w_n)$, and if the Doppler system is sensitive to the velocity component w, the probability distribution function for w_n is

$$p(w_n,\Delta t\ ;\ w_{n-1}) = \left[\frac{m}{2\pi kT\ (1-e^{-2\beta\Delta t})}\right]^{1/2} \exp\left[\frac{-m\ (w_n - w_{n-1}e^{-\beta\Delta t})^2}{2kT\ (1-e^{-2\beta\Delta t})}\right] . \tag{2.8}$$

2.2 Measurement of Brownian Motion With a LDV System

Consider a cross-beam laser Doppler velocimeter system, operating in fringe mode,[2.2] set up to measure the velocity of a particle in Brownian motion. For a perfect detection system as a whole, the transfer function is shown in Figure 2.3. The transfer function is the relationship between the input quantity of interest, the position of the particle in Brownian motion, and the output signal, which is the beat amplitude of the two fringe forming laser beams as seen by a square-law detector.

$$\text{signal} \sim \left\langle\left|\mathrm{Re}(\underline{E}_1 e^{i\underline{k}_1\cdot\underline{r}} + \underline{E}_2 e^{i\underline{k}_2\cdot\underline{r}})\right|\right\rangle \tag{2.9}$$

$$\sim 1 + \cos\ (\Delta\underline{k}\cdot\underline{r})$$

In the normal LDV application, the particle traverses the illuminated volume with a constant velocity (from A to B in Figure 2.3). If u is the velocity component in the direction of $\underline{k}_1 - \underline{k}_2$,

$$\Delta\hat{\underline{k}}\cdot\underline{r} = ut, \tag{2.10}$$

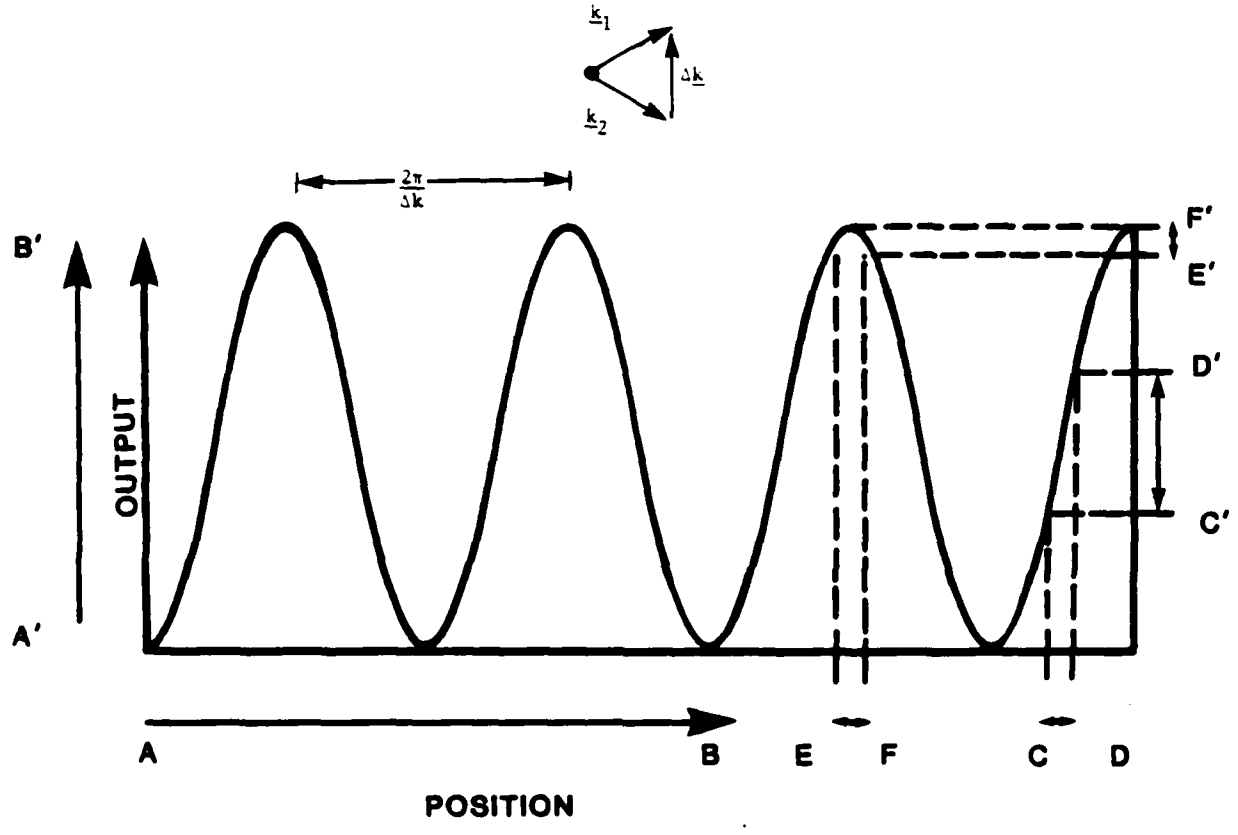

Figure 2.3 Transfer Function of Laser Doppler Velocimeter System.

the signal will be modulated fully (A'B') as

$$\text{signal} \sim 1 + \cos(\Delta k u t) \tag{2-11}$$

and the velocity may be obtained from the period τ of the modulation,

$$u = 2\pi/\Delta k\, \tau \tag{2.12}$$

Note that implicit in this velocity measurement is a length scale $(\Delta k)^{-1}$ so that a time measurement (τ) can yield a velocity.

In the detection of Brownian motion, however, u is a statistical quantity which changes rapidly in time. In particular, the particle may change velocity appreciably (or may even reverse its direction) before it traverses a "fringe" of the transfer function. On the average, the "excursion" of the particle is

$$\langle z \rangle_{rms} \sim \tau_{relax} \sqrt{(kT/m)} \tag{2.13}$$

The values of $\langle z \rangle_{rms}/\lambda$ are shown in Figure 2.4. The average excursion is smaller than the fringe spacing $2\pi/\Delta k$, therefore the signal is no longer fully modulated and $(\Delta k)^{-1}$ ceases to be a relevant length scale. Because of the nonlinear nature of the transfer function, the amplitude of the signal will not carry meaningful information. For example, when the particle oscillates about CD in Figure 2.3, the signal response C'D' is quite different from that (E'F') of a similar oscillation EF.

The only meaningful information contained in the signal is the time between the extrema of the signal modulation. Each extremum of the signal represents a reversal in direction of the particle, and therefore, a zero of the Brownian velocity u. In order to interpret the signal, it is necessary to examine the statistical distribution of the zeros of u. This procedure will

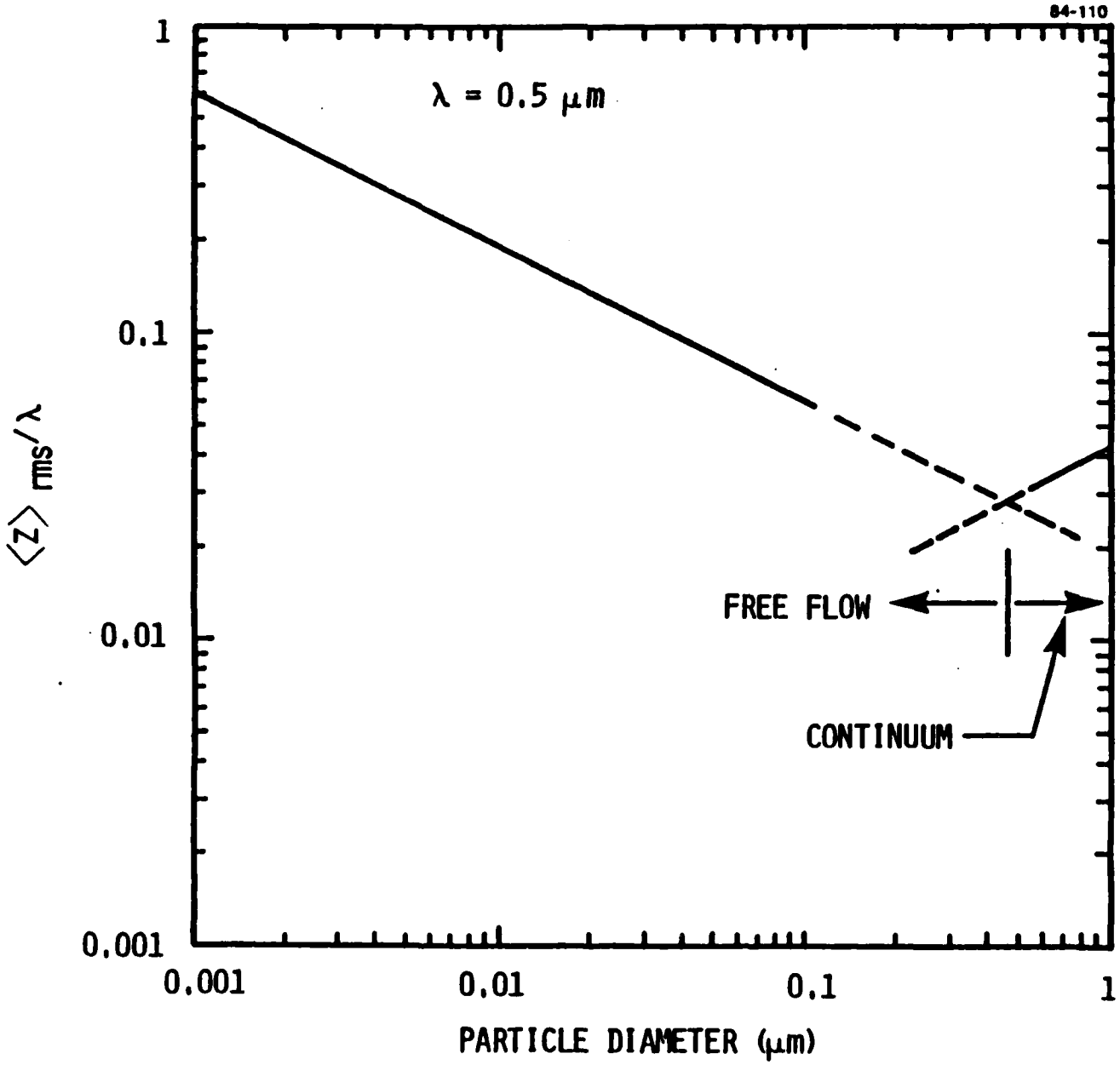

Figure 2.4. Mean Excursion Distance, Compared with the Wavelength of Visible Light, for Particles (Specific Gravity = 2) in Brownian Motion in a Gas at T = 300 K, p = 1 Atmosphere.

be described in Chapter 3. From the statistics, the relaxation time of the particle may be determined, and then the size information may be determined from Eq. (2.4) or (2.5).

2.3 References for Chapter 2

2.1 S. Chadrasekhar, "Stochastic Problems in Physics and Astronomy," in Review of Modern Physics, Vol. 15, 1943, pp. 1-89.

2.2 F. Durst, A. Melling, J.H. Whitelaw, Principles and Practice of Laser-Doppler-Anemometry, London, Academic Press, 1976.

3. SIMULATION OF THE BROWNIAN MOTION DOPPLER SIGNAL AND SIGNAL PROCESSING STRATEGY

In this chapter, a numerical simulation of the Doppler velocimeter signal from a particle in Brownian motion is reported. The simulation was based on a Monte Carlo technique for calculating the motion of the particle from the stochastic solution of the Langevin equation [Eq. (2-8)]. This motion was then coupled into the response of a laser Doppler velocimeter system operating in fringe mode to produce the Doppler signal. Then the results from using different methods for processing the signal were compared to formulate a signal processing strategy for the determination of the particle relaxation time.

3.1 Simulation of the Brownian Velocity

The measurement approach utilizes a laser interferometric system for measurement of an interference signal which is sensitive to the particle displacement. Such a system is shown schematically in Figure 3.1. This approach, in simple terms, is to measure the time-dependent interference signal arising from a single submicron particle ($\leq$ 0.1 μm diameter) passing through the measurement volume formed by the intersection of the laser beams in Figure 3.1 and to determine the particle size by statistical analysis of the signal. Although the system shown is physically similar to the familiar laser Doppler velocimeter, important differences in its implementation form the basis of the present approach. As explained in Chapter 2, the Doppler signal obtained from the scattered light only contains time (but not velocity) information which must be analyzed in a statistical sense. This concept is that the mean excursion distance for the particles in Brownian motion is much smaller than the wavelength of visible light, as shown in Figure 2.4. As

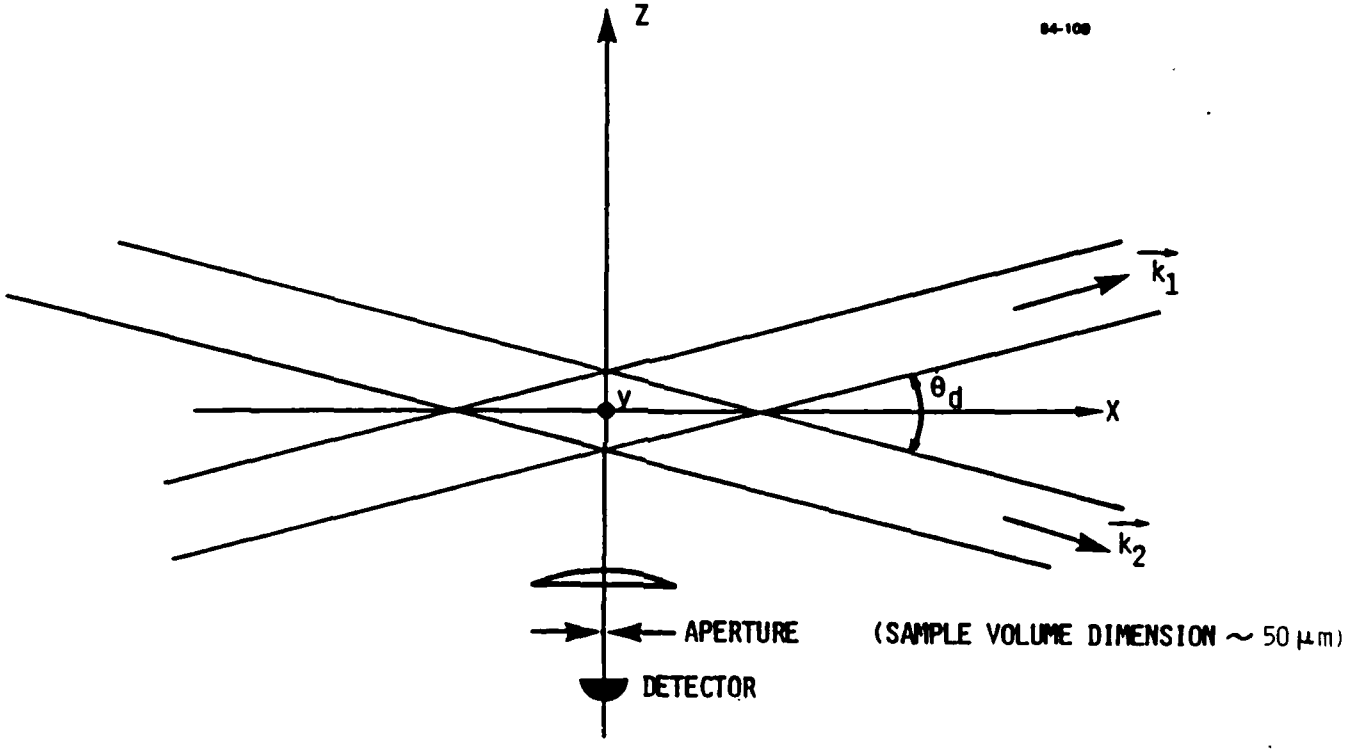

Figure 3.1. Laser Interferometric System for Measurement of Brownian Motion.

discussed in greater detail in Chapter 2, the consequence of this characteristic of the measurement is that the magnitude of signal variations is not meaningful (because the motion may be occurring in different regions of the LDV fringe pattern). The frequency characteristics of the signal are significant, however, in that they can be related to the statistics of particle motion. The identification of such relationships is the motivation for the computer simulation of the signal.

The basis of the computer simulation is the probabilistic solution (Eq. 2.8) of the Langevin equation. Using the probability distribution of Eq. (2.8), we may generate, using a pseudo-random number generator, the velocity history of w with the correct statistical properties. In general, if R is a random number with uniform distribution in the interval [0,1], and p(x) is the probability distribution of a variable x, R may be mapped into x by equating the probability of finding x in $[x_1, x_2]$,

$$\int_{x_1}^{x_2} p(x)\, dx = \int_{R_1}^{R_2} 1\, dR = R_2 - R_1 \quad . \tag{3.1}$$

In particular let $x_1 = -\infty$ and $R_1 = 0$; then

$$\int_{-\infty}^{x} p(x)\, dx = \int_{0}^{R} 1\, dR = R \quad . \tag{3.2}$$

For the distribution of Eq. (2.8), it is convenient to rewrite the expression as

$$p\,(w_n, \Delta t;\, w_{n-1}) = \frac{A}{\sqrt{\pi}} \exp\left[-A^2 (w_n - w_{n-1} h)^2\right] \tag{3.3}$$

where

$$A^2 = \frac{m}{2kt(1-h^2)} \tag{3.4}$$

$$h = e^{-\beta \Delta t} \quad . \tag{3.5}$$

Then Eq. (10) becomes

$$\frac{A}{\sqrt{\pi}} \int_{-\infty}^{w_n} \exp\left[-A^2(w_n - w_{n-1}h)^2\right] dw = R \quad , \tag{3.6}$$

from which w_n may be solved from the random number R. The solution of Eq. (3.6) is

$$w_n = \frac{\xi_n}{A} + w_{n-1}h \quad , \tag{3.7}$$

where

$$\xi_n = \text{erf}^{-1}(2R_n - 1) \quad . \tag{3.8}$$

To summarize, the algorithm for generating the Brownian velocity history works as follows. The initial velocity w_1 is obtained randomly from the Maxwellian distribution

$$p(w_1) = \left(\frac{m}{2\pi kt}\right)^{1/2} \exp\left(\frac{-mw^2}{2kt}\right) \quad , \tag{3.9}$$

or

$$w_1 = \left(\frac{2\pi kt}{m}\right)^{1/2} \text{erf}^{-1}(2R_1 - 1) \tag{3.10}$$

The subsequent velocities w_n, with sampling time Δt, are then given by Eqs. (3.7) and (3.8).

3.2 The Doppler Signal

Consider a crossed laser beam system with beam waist r_o as shown in Figure 3.1. The intensities of the two beams scattered by the particle at $\underline{x} = (x,y,z)$ (in a coordinate system centered on the probe volume) are

$$I_1 \sim \frac{\exp\left[- \left| \underline{x} - (\underline{x} \cdot \hat{\underline{k}}_1)\hat{\underline{k}}_1 \right|^2 \right]}{r_o^2} \tag{3.11}$$

$$I_2 \sim \frac{\exp\left[- \left| \underline{x} - (\underline{x} \cdot \hat{\underline{k}}_2)\hat{\underline{k}}_2 \right|^2 \right]}{r_o^2} \tag{3.12}$$

Here the unit propagation vectors are

$$\hat{\underline{k}}_1 = \left(x \cos\frac{\theta_d}{2}\ ,\ 0,\ -z \sin\frac{\theta_d}{2}\right)$$

$$\hat{\underline{k}}_2 = \left(x \cos\frac{\theta_d}{2}\ ,\ 0,\ z \sin\frac{\theta_d}{2}\right) \quad . \tag{3.13}$$

Therefore the expressions for I_1 and I_2 become

$$I_{\frac{1}{2}} = \frac{\exp\left[-\left(x \sin^2 \frac{\theta_d}{2} \pm z \sin \frac{\theta_d}{2} \cos \frac{\theta_d}{2}\right)^2 + y^2 + \left(z \cos^2 \frac{\theta_d}{2} \pm x \cos \frac{\theta_d}{2} \sin \frac{\theta_d}{2}\right)^2\right]}{r_o^2} \tag{3.14, 3.15}$$

The mean particle trajectory is

$$\underline{x}(t) = \underline{x}_o + \bar{\underline{v}}\, t \quad , \tag{3.16}$$

where $\underline{x}_o$ is the reference point and $\bar{\underline{v}}$ is the mean velocity. Substitution of $\underline{x}(t) = (x(t), y(t), z(t))$ from Eq. (3.16) into Eqs. (3.11) and (3.12) would give the scattered intensity profile as the particle traverses the beam volume.

At the detector, because of the interference between the two beams, the light collected is a modulated Doppler signal. The signal may be written as

$$S \sim I_1 + I_2 + 2\sqrt{I_1 I_2} \cos\left(\Delta k_z \cdot \int^t v_z dt + \phi\right) \quad , \tag{3.17}$$

where

$$\Delta k_z = \frac{2\pi}{\lambda}\left(2 \sin \frac{\theta_d}{2}\right) \quad , \tag{3.18}$$

and the z velocity component contains both a mean and random velocity,

$$v_z = \bar{v}_z + w(t) \quad . \tag{3.19}$$

The phase shift ϕ is a constant depending on the reference point definition.

The power received at the detector may therefore be written as

$$P = \left(\frac{I_o}{2} H \int \frac{d\sigma}{dr}\, dr\right)$$

$$\cdot \left\{f_1 + f_2 + 2\sqrt{f_1 f_2} \cos\left(\frac{2\pi}{\lambda} \cdot 2 \sin\frac{\theta_d}{2} \cdot \left[\bar{v}_z\, t + \int_{-\infty}^{t} w(t)dt\right]\right)\right\} \quad . \tag{3.20}$$

The first term represents the absolute intensity function which is proportional to the beam intensity I_o, the aperture and transmissivity function H of the receiving optics, and the scattering cross-section integrated over the appropriate field of view. The functions f_1 and f_2 are defined by the right hand sides of Eqs. (3.11) and (3.12). The cosine term represents the heterodyned Doppler signal.

3.3 Simulation Results and Discussion

The Brownian velocity of a 0.1 μm diameter spherical particle with a specific gravity of 2 in 300 K air at atmospheric pressure has been simulated using the Monte-Carlo calculation described above. The velocity history is shown in Figure 3.2 for 500 velocity samples with a sampling time of 10 ns each. The velocity statistics are shown in the histogram in Figure 3.3. The result agrees with the Maxwellian distribution which is also plotted in the figure.

Calculations were then carried out to examine the behavior of the Doppler signal, which is described by Eq. (3.20). The term of interest is

$$S = \frac{1}{2}\left\{f_1 + f_2 + 2\sqrt{f_1 f_2} \cos\left(\frac{2\pi}{\lambda} \cdot 2 \sin\frac{\theta_d}{2} \left[v_z t + \int_{-\infty}^{t} w(t)dt\right] + \phi\right)\right\} \quad , \tag{3.21}$$

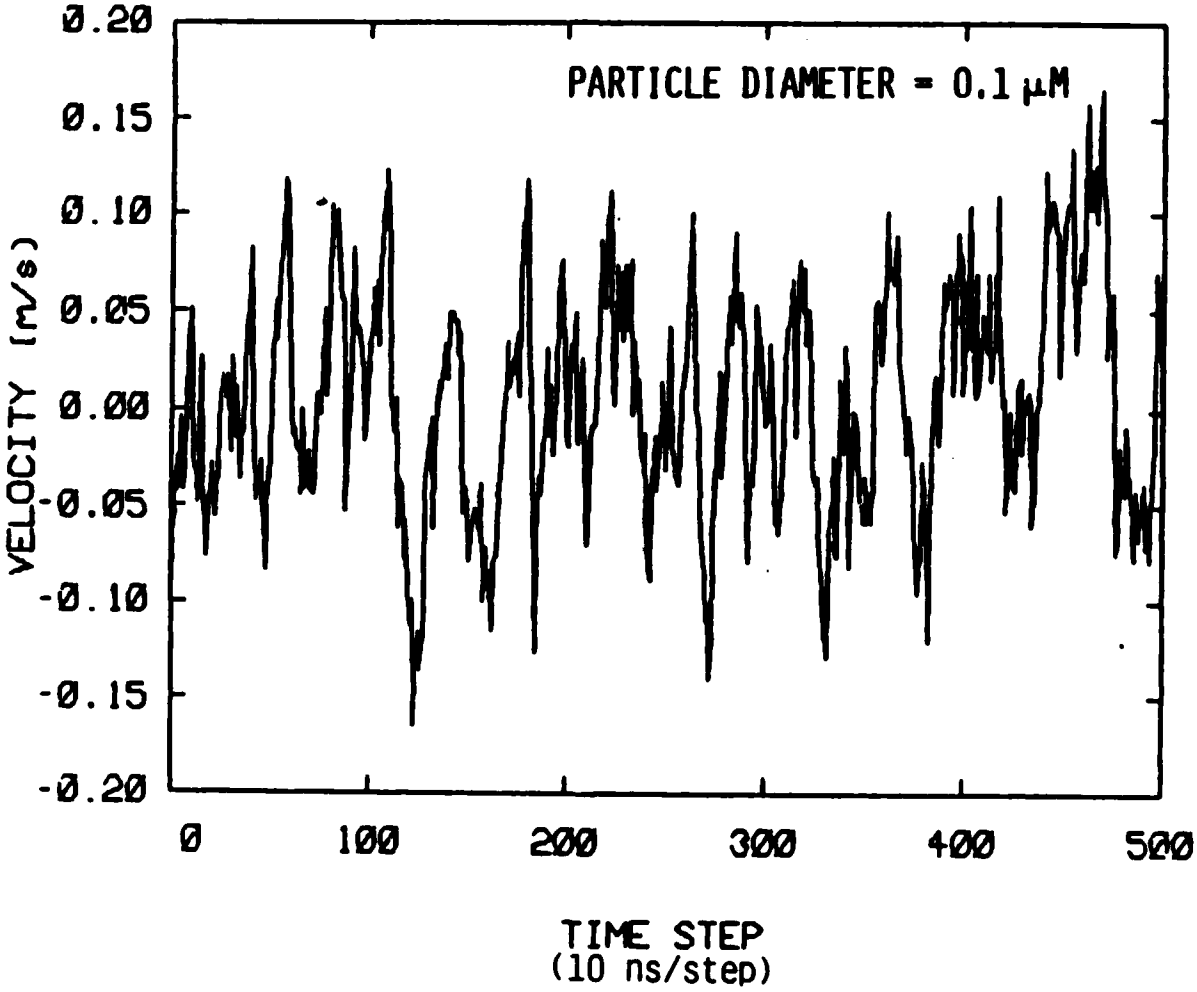

Figure 3.2. Simulated Brownian Velocity History of a 0.1 μm Diameter Particle (Specific Gravity = 2) in Air at T = 300 K, p = 1 atm

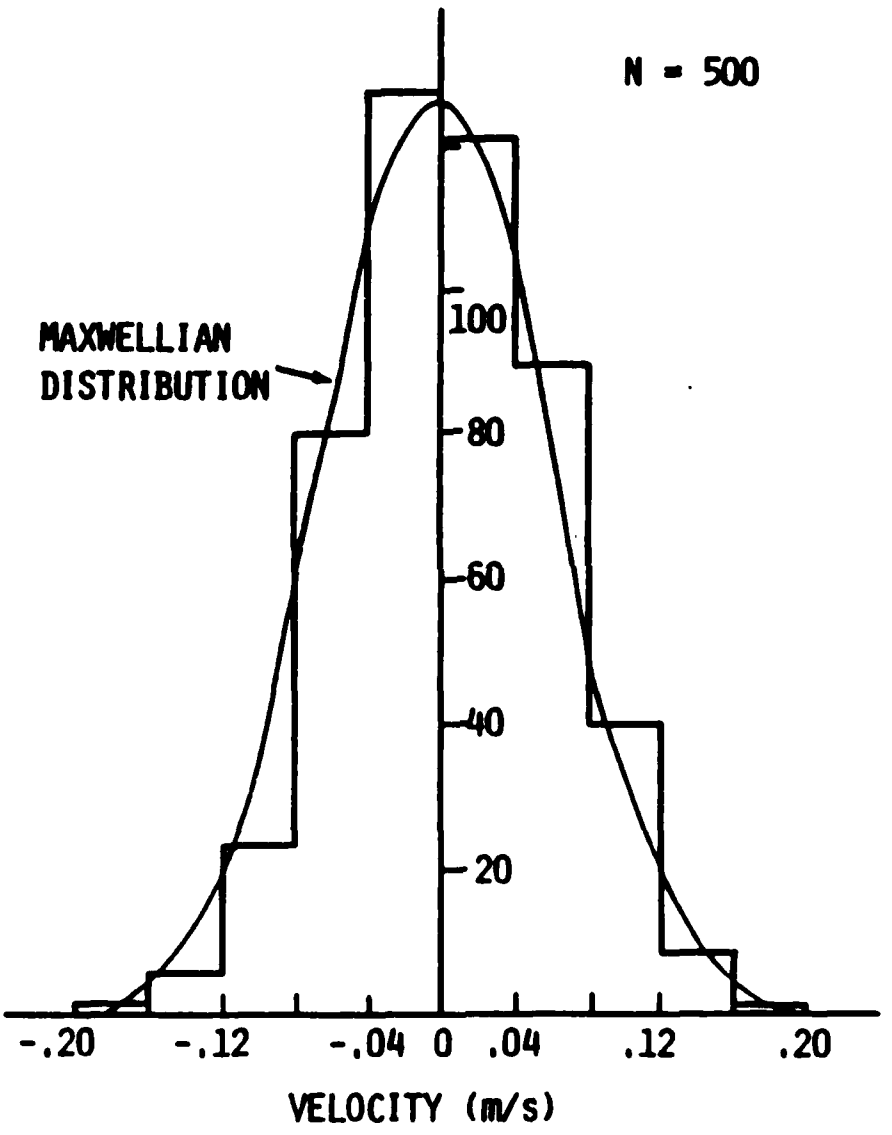

Figure 3.3. Comparison of the Velocity Distribution Obtained from the Monte Carlo Simulation with a Maxwellian Distribution

with f_1 and f_2 defined by the right hand sides of Eqs. (3.11) and (3.12). To obtain the most favorable signal, the particle is assumed to have mean velocity in the y direction only, and is traversing the center of the sample volume along the y axis. The reference phase value is set arbitrarily to (-0.5π) which corresponds to aligning the y axis along the "boundary" of the bright and dark fringes in the beam sample volume. The laser beam waist r_o is 50 μm and the beam crossing angle is set at $\theta_d = 10°$. These values are typical of a practical system.

Under the above conditions, the simulated Doppler signal for a 0.1 μm particle with $v_y = 1\ m \cdot s^{-1}$ traversing the center part of the beam volume, starting from $\underline{x}$ = (0., -10 μm, 0.), is shown in Figure 3.4(a). The horizontal axis is the number of time steps, with each time step equal to 10 ns. The signal fluctuation due to the Brownian motion is clearly detectable.

The simulation is repeated, under the same conditions, with a 0.01 μm diameter particle. The simulated signal for the smaller particle is shown in Figure 3.4(b). The fluctuation is of a much higher level than those exhibited by the larger diameter particle. Furthermore, because of the behavior of the cosine function, the modulation is reduced when the argument of the cosine is close to $\pm n\pi$, n = 0,1,2,.... For the signal in Figure 3.4(b), the particle is very close to the center of the beam volume as the absolute intensity is approximately constant. Therefore, the signal has a magnitude of

$$S \sim 1 + \cos\left\{\frac{2\pi}{\lambda} \cdot 2 \sin\frac{\theta_d}{2}\left[\bar{v}_z t + \int w(t)dt\right] + \phi\right\} \quad . \qquad (3.22)$$

Thus, at regions where S ~1 or 2, the magnitude of the modulation is reduced. This effect is evident in Figure 3.4(b).

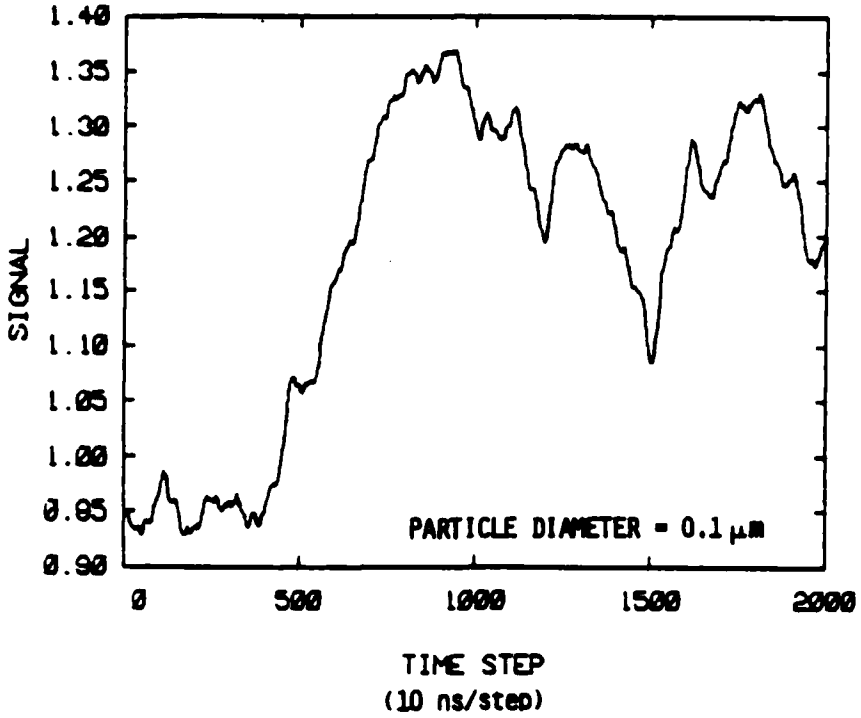

(a)

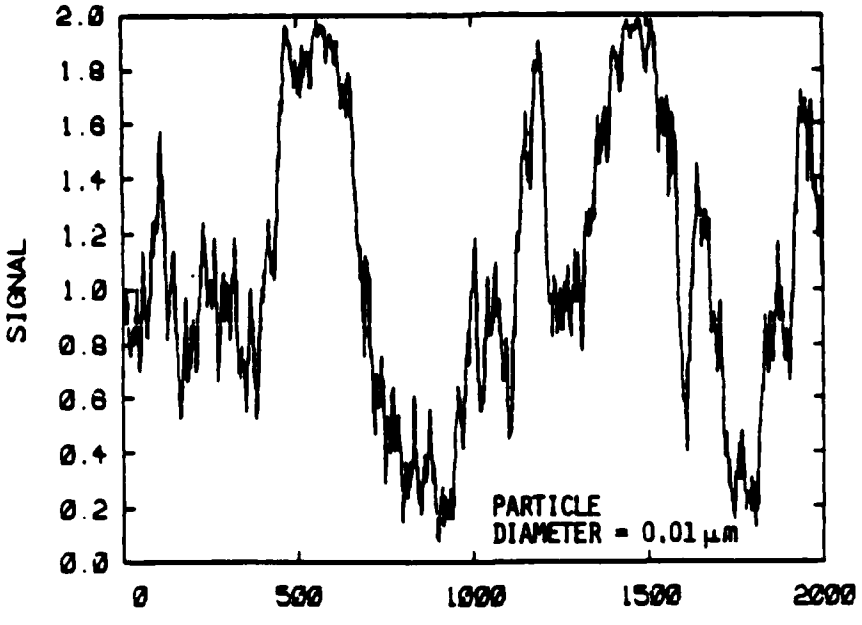

Figure 3.4. Simulated Time Dependent Interference Signals:
(a) 0.1 μm Diameter Particle
(b) 0.01 μm Diameter Particle

The signal modulation in Eq. (3.21) is a result of the cosine term, which is rewritten here as

$$\text{modulation} \sim \cos(k'z + \phi) \tag{3.23}$$

where

$$k' = \frac{2\pi}{\lambda} \cdot 2 \sin \frac{\theta}{2} \tag{3.24}$$

and

$$z = \bar{v}_z t + \tilde{z} \tag{3.25}$$

$$\tilde{z} = \int^t w(t)dt \quad . \tag{3.26}$$

The root-mean-square value $\langle\tilde{z}\rangle_{rms}$ of the Brownian displacement is shown in Figure 3.5. For particles of 100 to 1000 Å diameter, $\langle\tilde{z}_m\rangle/\lambda \sim 0.1$. Therefore the rms displacement is much less than the fringe spacing k'^{-1}. As a result, the length scale λ does not play any role in the determination of the Brownian velocity w. The signal, therefore, only contains information about the time scale and not any length scale, and the determination of a meaningful velocity is, in principle, not possible.

The essence of the above discussion is illustrated in Figure 3.6, which exhibits the transfer function of the detection system [the right hand size of Eq. (3.31)]. For typical Brownian motion modulation (AB), the signal modulation is (A'B'). The signal modulation is drastically reduced where the slope of the transfer function vanishes (CD). The amplitude of the modulation is a function of the position of the particle relative to the fringe pattern. Since this is not known a priori, the amplitude modulation, therefore, does not provide useful information on the nature of the Brownian motion.

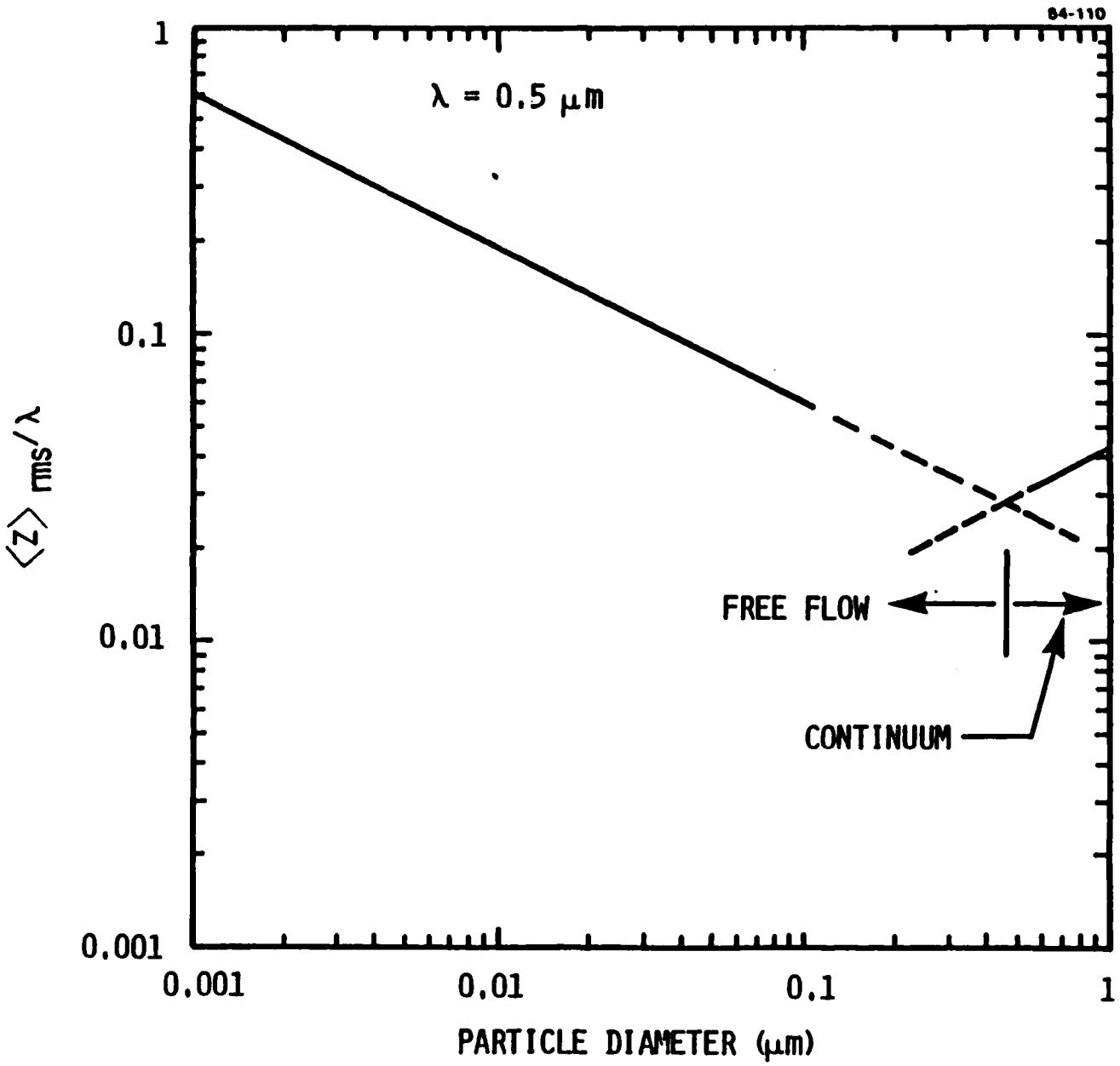

Figure 3.5. Mean Excursion Distance, Compared with the Wavelength of Visible Light, for Particles (Specific Gravity = 2) in Brownian Motion in a Gas at T = 300 K, p = 1 Atmosphere

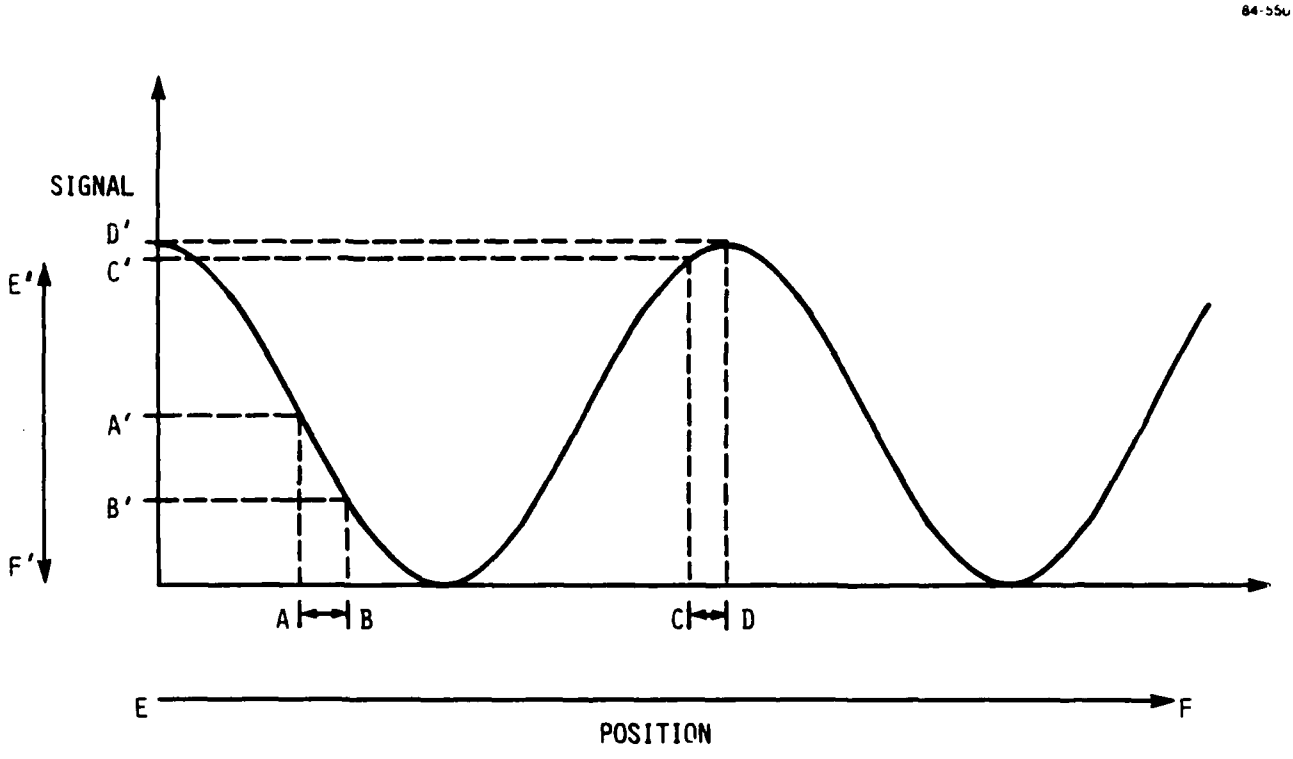

Figure 3.6. Modulation of the Doppler Signal as a Function of Particle Position

When there is a fluid velocity component $\bar{v}_z$ perpendicular to the fringe pattern, the particle position will be represented by the trajectory (EF), with the Brownian modulation such as (AB) superimposed on top. The signal will exhibit full modulation (E'F') (regular Doppler signal) with the Brownian motion modulation (A'B') superimposed on top. When $\bar{v}_z$ is large compared to the Brownian velocity w, it may be difficult to recover the Brownian motion modulation from the regular Doppler signal. This effect is illustrated in Figures 3.7(a) and 3.7(b) in which velocity $\bar{v}_z$ of 0.1 and 0.3 $m \cdot s^{-1}$ respectively are superimposed onto the Brownian velocity. In the latter case, the Brownian motion signal is almost completely masked and the signal resembles the usual Doppler velocimeter signal. For small particles with a higher Brownian velocity, good quality signal may still be obtained with a significant $\bar{v}_z$. This is illustrated in Figure 3.8 by the simulation of the signal from a 0.01 μm particle with $\bar{v}_z = 0.3$ $m \cdot s^{-1}$. The mean Brownian velocity $\bar{w}$, where

$$w = \sqrt{\frac{8kT}{\pi m}} \tag{3.27}$$

is approximately 0.1 $m \cdot s^{-1}$ for a 0.1 μm diameter particle at a gas temperature of 300 K. Thus one expects that for particles in the 0.01 to 0.1 μm diameter range, reasonable signal quality may be obtained if $\bar{v}_z$ is less than 0.1 $m \cdot s^{-1}$.

The above discussion indicates that the strategy for analyzing characteristics of the Brownian motion lies in analysis of the time information. The fundamental time scale of the fluctuation is the relaxation time $1/\beta$. The information on the particle size may be calculated from β using Eqs. (2.4) and (2.5). Furthermore, the signal must be filtered to remove the regular Doppler component ($\bar{v}_z$) for proper interpretation.

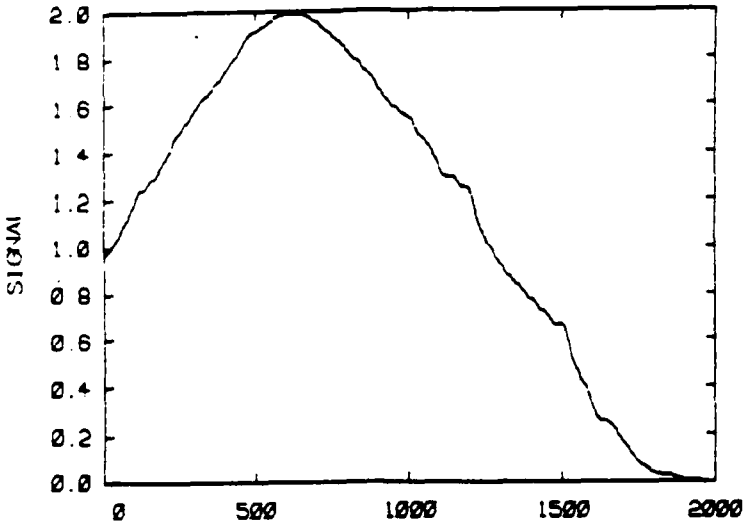

(a)

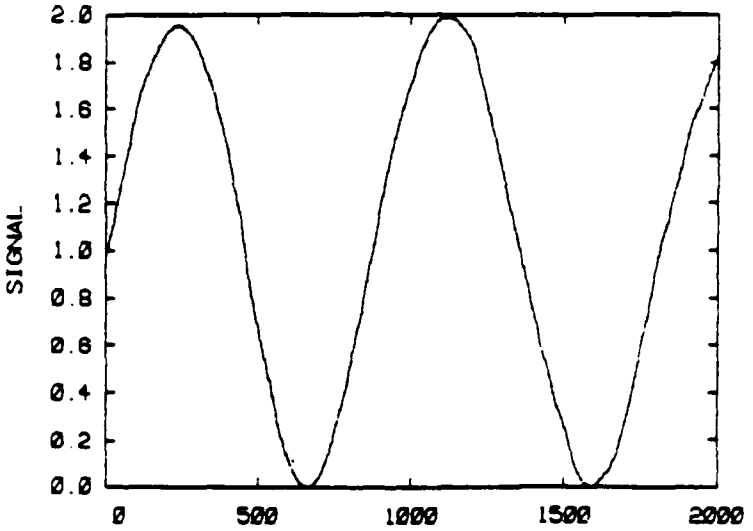

(b)

Figure 3.7. Simulated Brownian Motion Signals for a 0.1 μm Diameter Particle with Fluid Velocity Component $\bar{v}_z$ Superimposed

(a) $\bar{v}_z = 0.1$ m s^{-1}

(b) $\bar{v}_z = 0.3$ m s^{-1}

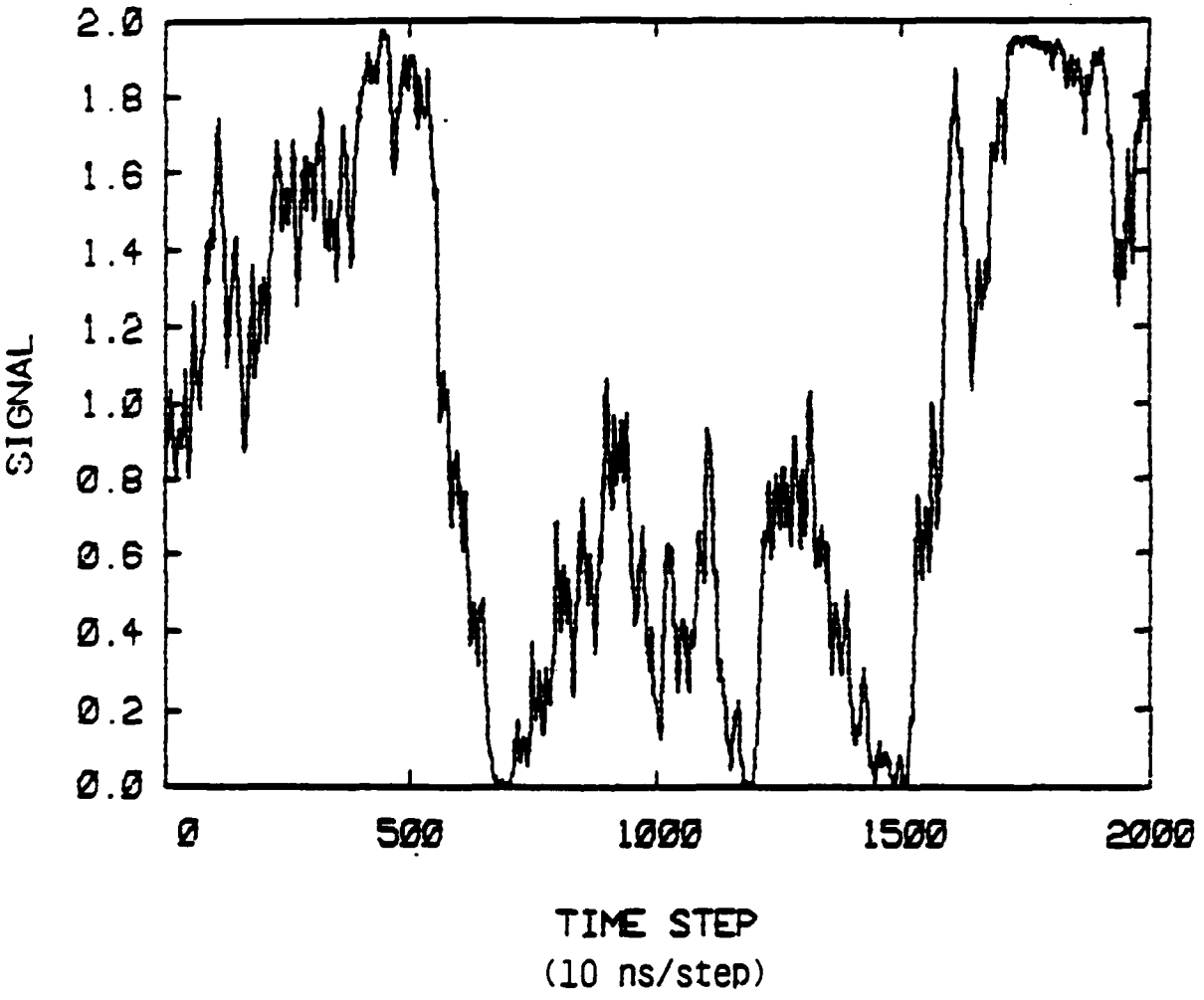

Figure 3.8. Simulated Brownian Motion Signal for a 0.01 μm Diameter Particle with $\bar{v}_z$ = 0.3 m s^{-1} Superimposed

3.4 Processing of the Brownian Motion Sensor Signal

As discussed above, only time information may be obtained from the Brownian motion sensor. Since the time scale relevant to the Brownian motion is much faster than any other time scales (e.g., the transit time of the particle due to its mean velocity), the latter may be filtered out easily. In the following discussion we shall assume that the signal has already been filtered to contain the Brownian information only. The appropriate statistics of the temporal information signal are discussed.

As depicted in Figure 3.6, the signal amplitude is a function of the absolute position of the particle within the probe beam volume. Therefore, the relevant information is contained in the time between the extrema of the signal. At an extremum, there is a change of direction of the particle, and, therefore, the extremum represents a zero crossing of the particle velocity. Thus, the Brownian motion may be analyzed in terms of the time between extrema of the signal (zero crossing of the first derivative). The particular method of implementation depends on the hardware configuration. Nevertheless the principle remains the same. Also, the analysis considers only the mean time between extrema, and does not to attempt analyze the full spectral content of the signal, so that possible aliasing is not an issue. (The method amounts to doing statistical sampling rather than fixed interval sampling, so on the average, the higher frequency content is "represented.")

The signal processing is simulated on the computer using the Monte Carlo technique described previously. The Brownian motion of a particle with specific gravity of two, embedded in room temperature air, is analyzed. The mean time between extrema $\bar{t}$ as a function of the particle diameter d is shown in Figure 3.9. The values of $\bar{t}$ do not seem to follow a simple linear relationship with d, yet the only time scale involved is the relaxation time $\tau_{relax} = 1/\beta$. With β proportional to 1/d in the free flow regime, the relaxation time should be proportional to d. Furthermore, depending on the sampling interval Δt, the mean time $\bar{t}$ is different. The relevant parameter

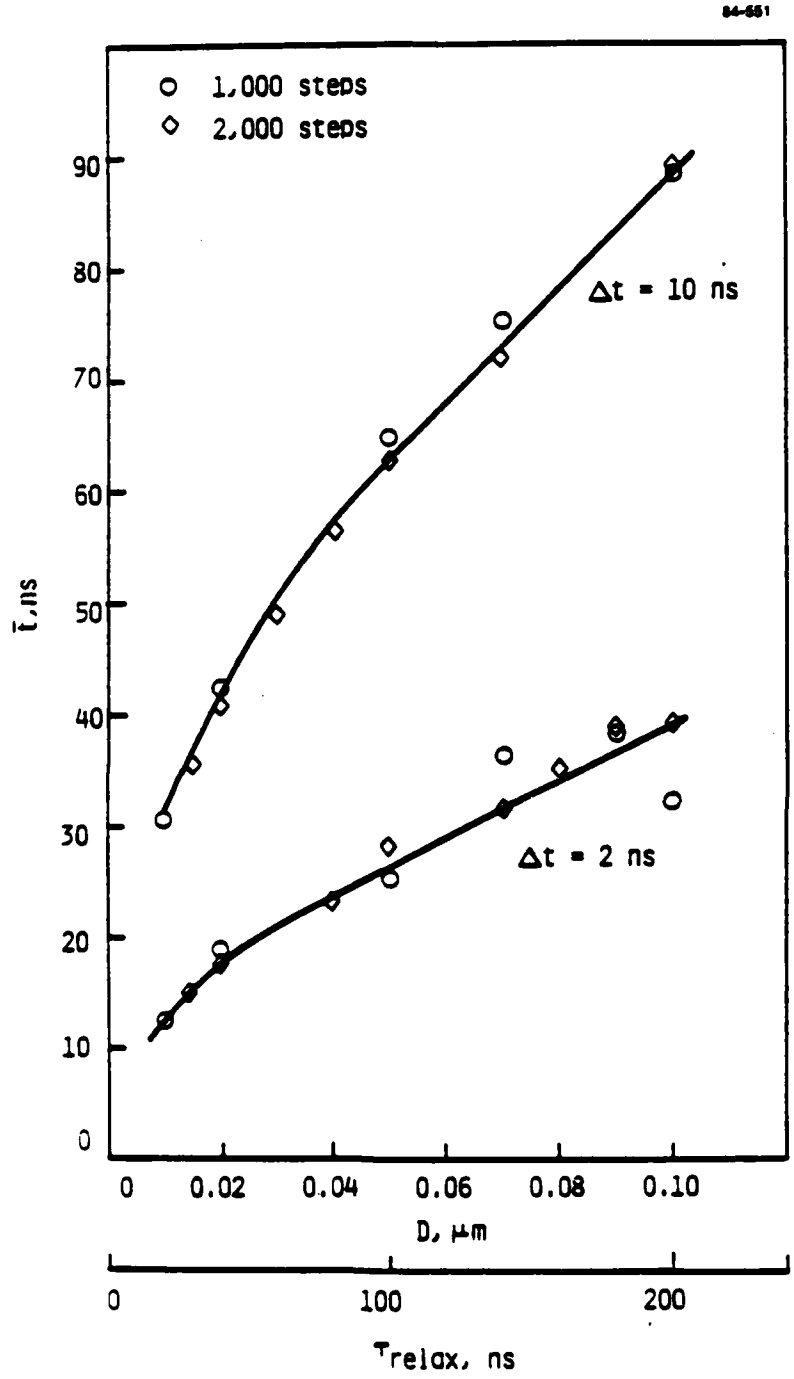

Figure 3.9. Mean Time Between Extrema in Brownian Motion Interference Signal, for Two Sampling Intervals

should therefore clearly involve Δt. This issue is resolved when the data are replotted against $\sqrt{\Delta t/\beta}$ (with the dimension of time) (Figure 3.10). The simulation points collapse on to a single straight line passing through the origin. The relationship between sampling and adequate statistics is also illustrated, at large values of $\sqrt{\Delta t/\beta}$, a long string of data is required to produce a good estimate of t. For small values of $\sqrt{\Delta t/\beta}$, the sampling interval of $\Delta t = 10$ ns is not adequate to resolve the Brownian motion time scale, and as a result, t is overestimated.

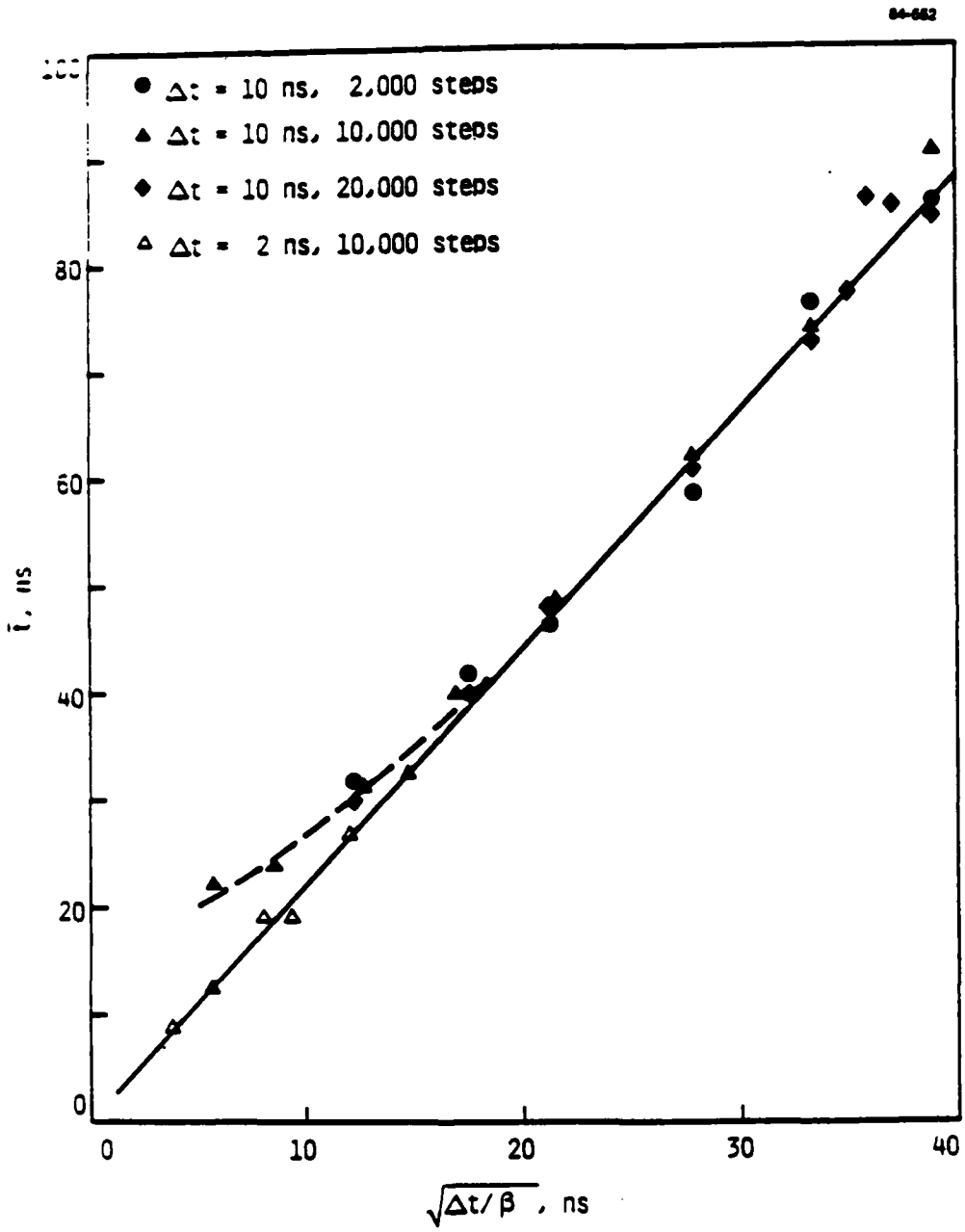

Figure 3-10. Correlation Between the Mean Time Between Signal Extrema and the Particle Relaxation Time, β^{-1}

4. THEORETICAL ANALYSIS OF THE DOPPLER SIGNAL

In the last section, a Monte Carlo simulation of the signal from the Brownian motion sensor was carried out. The result of interest, namely, the time between zero crossings of the Brownian velocity, was found to be dependent on the step size Δt of the simulation. This dependence is actually not surprising because Δt represents essentially the bandwidth of the actual signal detection system, which, being a practical device, should have a finite bandwidth. Since the Brownian motion is a statistical process, the behavior of any signal derived from the Brownian motion is statistical, and the spectral properties of the signal will depend on the bandwidth of the signal detection system. These ideas are further explored in this chapter. Also an analytical approach is attempted in order to provide a theoretical basis for the signal processing method used in Chapter 3.

4.1 The Statistical Nature of the Brownian Velocity

The Brownian velocity of a particle in thermal equilibrium in a background fluid is described by the Langevin equation (see Chapter 2). For the observed velocity component u (in the direction of $\Delta\underline{k}$), the Langevin equation is

$$\frac{du}{dt} + \beta u = f \tag{4.1}$$

where β^{-1} is a relaxation time governed by the mass m and the mobility ε of the particle in the fluid.

$$\beta = \frac{1}{\tau_{relax}} = \frac{\varepsilon}{m} \tag{4.2}$$

The statistical nature of u is due to the random driving force f, which is the result of the impulse arising from each collision of the particle and a molecule of the background fluid. Because these collisions occur randomly, f may be considered to be a white noise function with a constant spectral density S_f,

$$< f(t)f(t+\tau) > = S_f\delta(t) \tag{4.3}$$

The time scale associated with the fluctuation of f is of the order of the time between the molecular collisions τ_c, which, for a 0.1 μm particle in a gas medium at STP is approximately 10^{-14} s. The time response of practical instruments used to observe the Brownian motion velocity is usually much slower than this collision time. The observations, are, therefore, the result of averaging u over a response time scale Δt associated with the instrument, with $\Delta t \gg \tau_c$. The observed value of u is then a random variable, and, since it is the aggregate of many similar events, it has a Gaussian distribution, by the central limit theorem. If the particle has a velocity u_o at one instant of time, the conditional probability distribution of u at a time Δt later, (so that the value of u is the aggregate sum of all the collisions in Δt), is given by[4.1]

$$p\ (u,u_o;\Delta t) = \frac{1}{\sigma\sqrt{\pi}}\ \exp\ [-(u-u_o h)^2/\sigma^2] \tag{4.4}$$

$$\sigma = \frac{m}{2kT(1-h^2)} \tag{4.5}$$

Note that the distribution is parameterized by the "memory" factor h

$$h \equiv e^{-\beta\Delta t} \tag{4.6}$$

and the width σ. The observed velocity u(t) may be viewed as observations at discrete points in time, $t_n = n\Delta t$. When the time step Δt is large compared to the relaxation time ($\beta\Delta t \gg 1$), the velocities u_i are independent of each other, and each obeys a Maxwellian distribution at temperature T. In the Brownian motion sensor described here, since the velocity amplitude is not measured, all the information is contained in the measurement of the value of β. Therefore, the instrument response time Δt should be such that $\beta\Delta t < 1$. After β is determined, the particle physical properties (ε,m) may be determined from Eq. (4.2).

4.2 The Distribution of the Zeros of the Velocity

The Brownian motion sensor measures the time between successive zeros of the Brownian velocity u (in the direction of $\Delta\underline{k}$). The time history of the velocity values, u(t), as observed by an instrument with an integration time Δt, may be thought of as a time series u_n at time $n\Delta t$. From Eq. (4.4) the values of each u_n are governed by the probability distribution

$$p\,(u_n,\, u_{n-1},\, \Delta t) = \frac{1}{\sigma\sqrt{\pi}} \exp\left[- (u_n - u_{n-1}h)^2/\sigma^2 \right] \qquad (4.7)$$

where the u_{n-1} appears as a parameter. We want to determine the probability P(N) of obtaining a time between two successive zeros of $N\Delta t$.

The problem of determining the distribution of zeros of a random variable has been studied extensively in the context of shot noise in electronic devices, and in queueing theory. The classic review of the subject is given in Reference 4.2. We shall derive the expression for P(N) independently here. To connect our result to that in the literature of noise current, the random driving force f in Eq. (5) may be considered as the randomly arriving electron, and the observed "current" u is the result of two transfer functions (or filters) in series. The first transfer function is that associated with the Langevin equation. Formally

$$u(t) = \int_{-\infty}^{\infty} \frac{\hat{f}\, e^{-i\omega t}}{(\beta+i\omega)} \frac{d\omega}{2\pi} \tag{4.8}$$

where $\hat{f}$ is the Fourier Transform of f. Physically, this transfer function is due to the averaging of the effect of f by the damping of the particle in the fluid. The second transfer function is due to the averaging by the instrument. Therefore the overall transfer function is

$$u(t) = \frac{1}{\Delta t} \int_{t-\Delta t}^{t} dt' \int_{-\infty}^{\infty} \frac{\hat{f}\, e^{i\omega t'}}{(\beta+i\omega)} \frac{d\omega}{2\pi} \tag{4.9}$$

It should be noted that no closed form solutions for P(N) have been worked out, except for rather trivial cases. The difficulty is attributed [4.2] to the lack of an analytical solution to the N dimensional integral involved (see Eq. (4.10).

We shall derive the expression for P(N) here. The process of obtaining a successive zero in N steps may be described as the following. At time zero ($n = 0$), the particle has a very small velocity δu, which, within the amplitude resolution of the instrument, may be considered as zero. In the following argument, δu is taken as positive. The argument will be exactly the same if δu is negative. We shall define a zero-crossing event at $t = N\Delta t$, ($n = N$), as an event with velocity greater than zero at $t = (N - 1)\,\Delta t$, ($n = N - 1$), and velocity less than or equal to zero at $t = N\Delta t$. The time resolution of this definition of zero-crossing is Δt, and so the meaning of such an event for $N = 1$ is not precise. Then, the condition for occurrence of a successive zero in N time steps is to have the velocities be positive for

n = 1, ..., N-1; and the velocity be negative or equal to zero for n=N. Therefore

$$P(N) = \int_0^\infty du_1\, p\,(u_1, 0; \Delta t) \int_0^\infty du_2\, p\,(u_2, u_1; \Delta t) \cdots \tag{4.10}$$
$$\cdots \int_0^\infty du_{n-1}\, p\,(u_{n-1}, u_{n-2}; \Delta t) \int_{-\infty}^0 du_n\, p\,(u_n, u_{n-1}; \Delta t)$$

Using the formula for p in Eq. (4.7), and changing the variable from u to $\xi = u/\sigma$, the above probability becomes

$$P(N) = \left(\frac{1}{\sqrt{\pi}}\right)^N \int_0^\infty d\xi_1\, e^{-\xi_1^2} \int_0^\infty d\xi_2\, e^{-(\xi_2 - \xi_1 h)^2} \cdots \tag{4.11}$$
$$\cdots \int_0^\infty d\xi_{n-1} e^{-(\xi_{n-1} - \xi_{n-2} h)^2} \int_{-\infty}^0 d\xi_n e^{-(\xi_n - \xi_{n-1} h)^2}$$

Note that σ does not appear in this expression. This is because the zero-crossing time pertains to the zeros of the velocity, and is therefore independent of the velocity scale. (The value σ is a velocity scale measuring the width of the velocity distribution).

If the integration time Δt is large ($\beta \Delta t \gg 1$), h will approach zero and Eq. (4.11) reduces to a binomial process

$$P(N) = \left(\frac{1}{2}\right)^N \tag{4.12}$$

The average value of N is

$$\bar{N} = \sum_{N=1}^\infty NP(N) = \sum_{N=1}^\infty \frac{N}{2^N} = \frac{d}{dx}\left|_{x=1} \left(\sum_{N=1}^\infty \left(\frac{x}{2}\right)^N\right) = 2\right. \tag{4.13}$$

In this case, the data values corresponding to the successive zeros of the velocity become a completely random sequence, and do not contain information about h.

For small values of h, the multiple integral may be worked out as follows: An operator I_n is defined as

$$I_n\,(f(\xi_n)) \equiv \frac{1}{\sqrt{\pi}} \int_0^\infty d\xi_n\, e^{-(\xi_n - \xi_{n-1}h)^2}\, f(\xi_n) \tag{4.14}$$

The quantity ξ_{n-1} enters as a parameter in the above definition. Then

$$I_n\,(1) = \frac{1}{2}\,(1 + \frac{2}{\sqrt{\pi}}\,\xi_{n-1}h) + O(h^2) \tag{4.15}$$

$$I_n\,(\xi_n h) = \frac{1}{2}\,\frac{h}{\sqrt{\pi}} + O(h^2) \tag{4.16}$$

The expression for P(N), Eq. (4.11), after evaluating the last integral on the right hand side, becomes

$$P(N) = \frac{1}{2}\, I_1\, I_2 \cdots I_{N-1}\,(1 + \frac{2}{\sqrt{\pi}}\,\xi_{N-1}h) + O(h^2) \tag{4.17}$$

The expression (4.15) and (4.16) may be used repeatedly in (4.17). The first few expressions are:

$$P(N) = (\frac{1}{2})^2\, I_1 \cdots I_{N-2}\,[(1 - \frac{2h}{\pi}) + \frac{2}{\sqrt{\pi}}\,\xi_{N-2}h] + O(h^2)$$

$$= (\frac{1}{2})^3\, I_1 \cdots I_{N-3}\,[1 + \frac{2}{\sqrt{\pi}}\,\xi_{N-3}h] + O(h^2)$$

$$= \left(\frac{1}{2}\right)^4 I_1 \cdots\cdots I_{N-4} \left[\left(1 + \frac{2h}{\pi}\right) + \frac{2}{\sqrt{\pi}} \xi_{N-4} h\right] + O(h^2)$$

$$\vdots$$

$$P(N) = \left(\frac{1}{2}\right)^N \left[1 + (N-3)\frac{2h}{\pi}\right] + O(h^2);\ N \geq 2 \qquad (4.18)$$

The above expression is valid for $N \geq 2$. For $N = 1$, since the velocity at $n = 0$ is preconditioned to be = 0,

$$P(1) = \int_{-\infty}^{0} e^{-(\xi_1 - 0)^2} d\xi_1 = \frac{1}{2} \qquad (4.19)$$

Compared to the binomial distribution ($P(N) = 2^{-N}$), which is the limit for $h = 0$, $P(N)$ decreases with h for $N < 3$ and increases with h for $N > 3$. This result is illustrated in Figure 4.1. Since the velocity at $n = 0$ is zero, the velocity u_1 at $n = 1$ is sampled from a Gaussian centered at zero. The value of $P(N = 1)$ is the probability that this velocity is negative, and $P(1)$ is therefore 1/2. Say the velocity at $n = 1$ is $u_1 (> 0)$, then the velocity u_2 at $n = 2$ is sampled from a Gaussian centered at $u_1 h$. The probability of u_2 being negative is the shaded area in Figure 4.1 under the Gaussian at $n = 2$, and this value is $< 1/2$ for $h > 0$. Therefore $P(2) < (1/2)^2$. For $N = 3$, the probability of obtaining a consecutive zero here is represented by the shaded area under the Gaussian centered at $u_2 h$ at $n = 3$ (Figure 4.1). This area has to be summed over all the realizations of the possible values of positive u_2, which is sampled from the Gaussian centered at $u_1 h$, which again has to be summed over all the realizations of u_1. Although the shaded area at $n = 3$ is less than 1/2, there are "more" realizations than

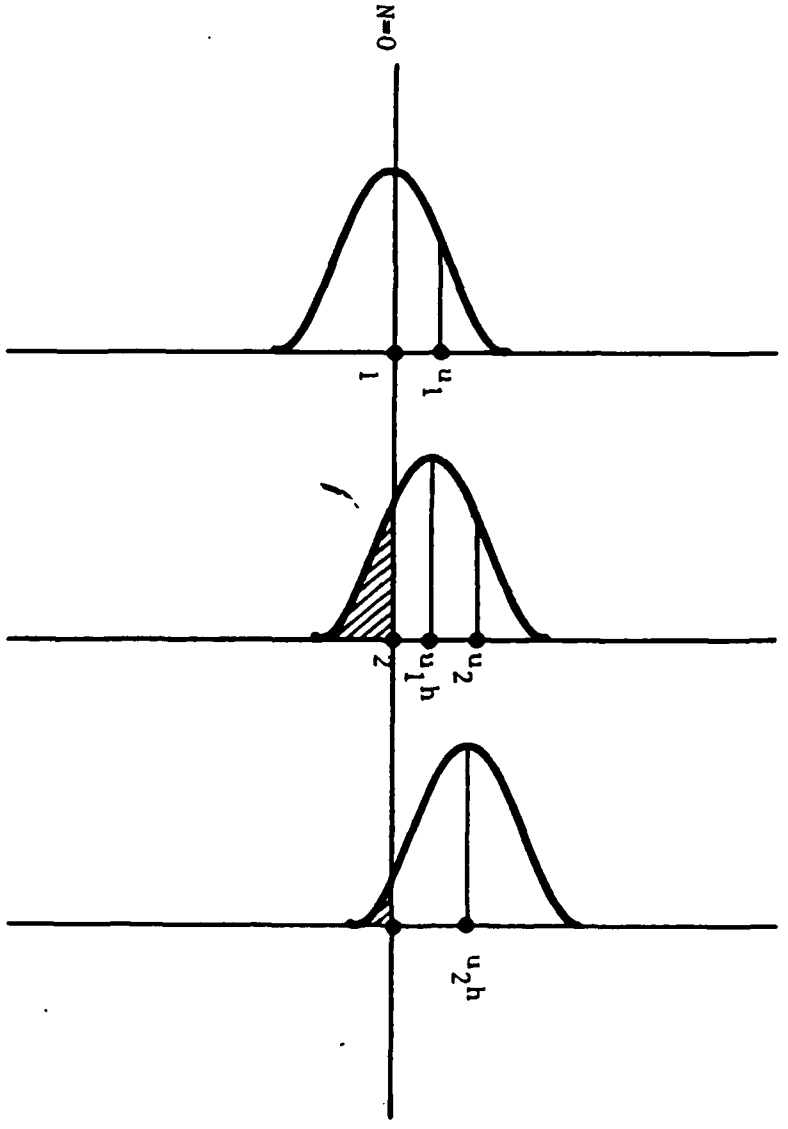

Figure 4.1 Velocity Sampling at the First 3 Time Steps.

the h = 0 case because u_2 is sampled from the shifted Gaussian. These two effects balance each other to $O(h^2)$, and P(3) is equal to $(1/2)^3 + O(h^2)$. For N > 3, P(N) is given by Eq. (22), and is greater than $(1/2)^N$. The values of P(N) are plotted versus N in Figures 4.2 and 4.3.

It is not possible to obtain a closed form solution of P(N) for arbitrary h ($h < 0 < 1$ corresponding to $0 < \beta\Delta t < \infty$) because of the difficulty in evaluating the multiple integral in Eq. (4.7). Direct numerical calculation the integral is not feasible for any large N, say N > 5. Monte Carlo evaluation of the integral would be equivalent to our earlier simulation of the Brownian motion in Chapter 3. The results of Chapter 3 will be reexamined in this context here.

The general behavior of the mean number of steps $\bar{N}$ between consecutive zero-crossings of the Brownian velocity is shown in Figure 4.4. For h = 0, $\bar{N}$ is 2 (from Eq. (4.13)). For small h,

$$\bar{N} = \sum_{N=1}^{\infty} N \left(\frac{1}{2}\right)^N \left(1 + (N-3)\,\frac{2h}{\pi}\right) + O(h^2)$$

$$= \sum_{N=1}^{\infty} \left(\frac{N}{2^N}\right) \left(1 - \frac{6h}{\pi}\right) + \sum_{N=1}^{\infty} \left(\frac{N^2}{2^N}\right) \left(\frac{2h}{\pi}\right) + O(h^2)$$

$$\bar{N} = O(h^2) \tag{4.20}$$

In the last expression, we made use of $\sum(N/2^N) = 2$ and $\sum(N^2/2^N) = 6$. Therefore $\bar{N} = O(h^2)$ for small h. For large relaxation time ($\beta \to 0$, $\beta\Delta t \to 0$, and $h \to 1$), the particle, once it acquires a positive (or negative) velocity, will retain that velocity for a large time. Consequently $\bar{N} \to \infty$.

The results of the Monte Carlo simulation in Chapter 3 have been replotted in the context of the present analysis in Figure 4.5, and confirm the theory. The results in Figures 4.4 and 4.5 show that to obtain h, (and

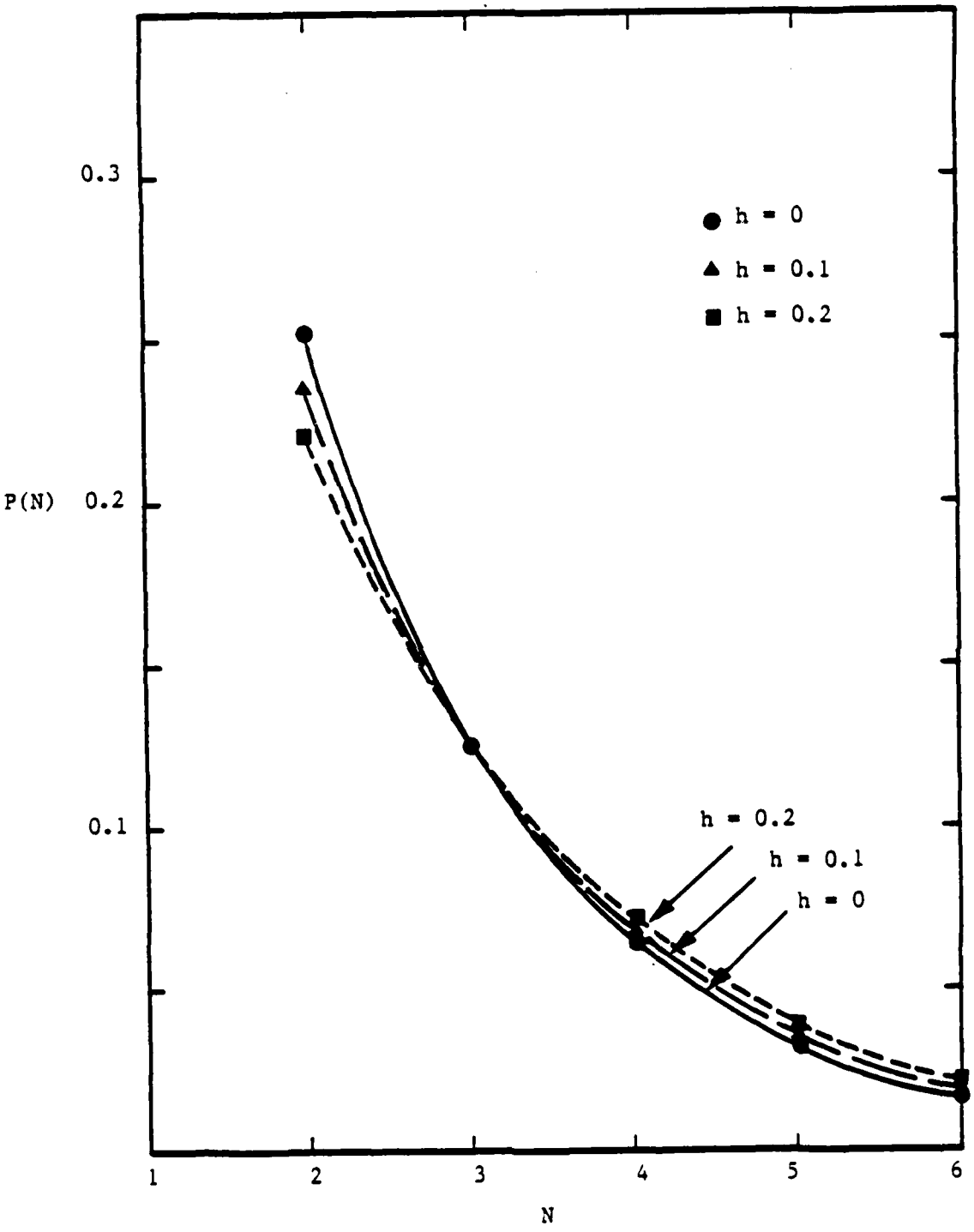

Figure 4.2 Probability of Obtaining a Consecutive Zero of the Brownian Velocity in N Steps (Linear Scale).

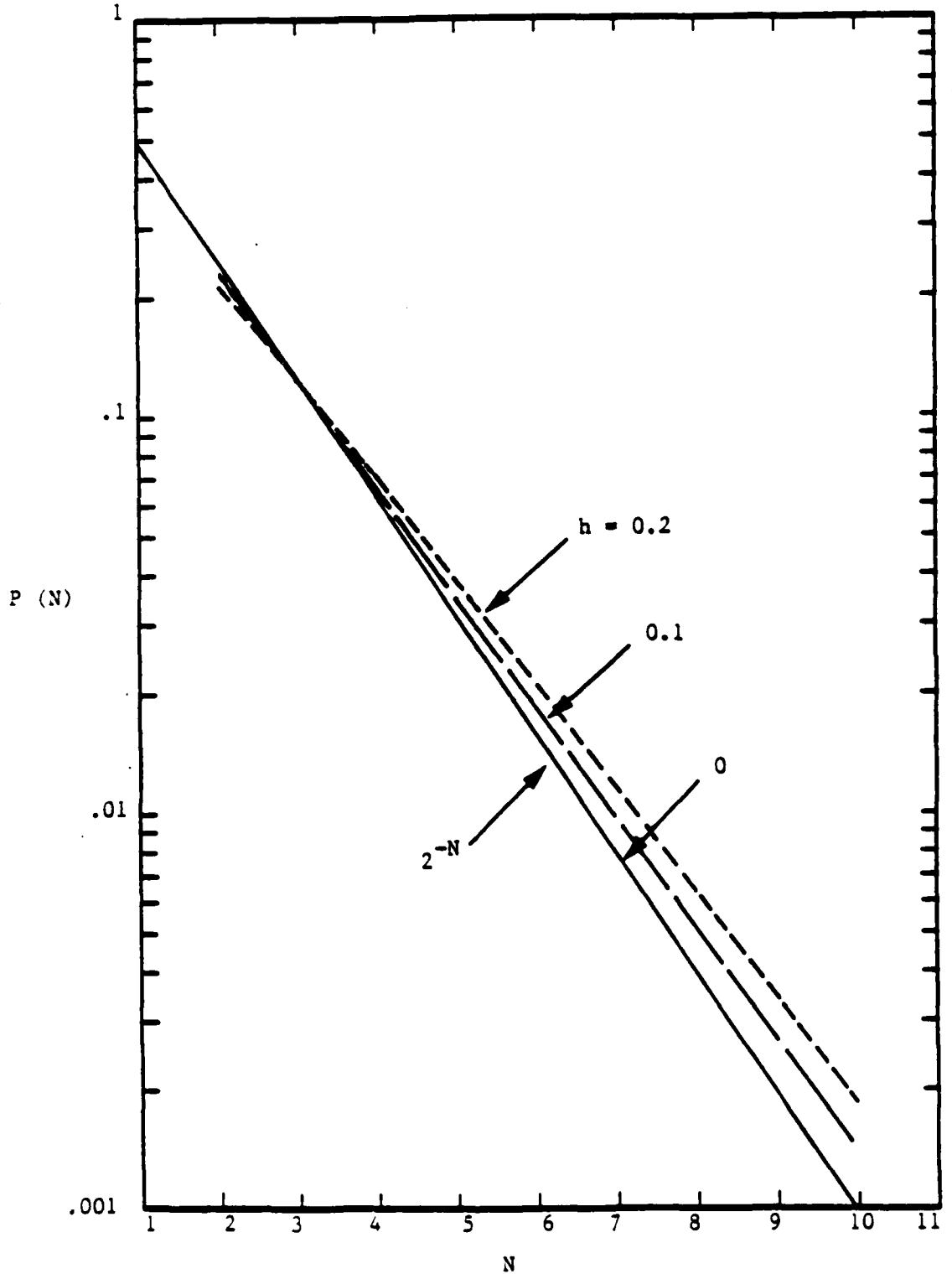

Figure 4.3. Probability of Obtaining a Consecutive Zero of the Brownian Velocity in N Steps (Semi-Log Scale).

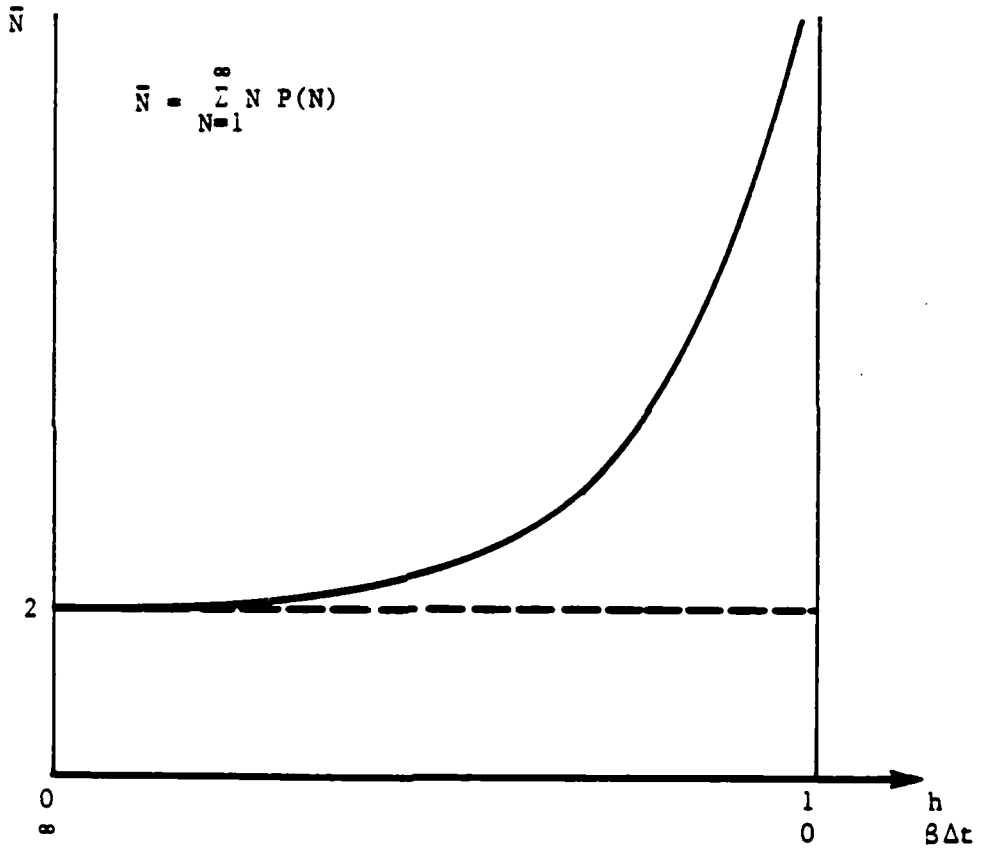

Figure 4.4. General Behavior of the Expectation Value of the Number of Time Steps Between Consecutive Zero-Crossings of the Brownian Velocity, as a Function of the Memory Parameter $h = \exp(-\beta\Delta t)$.

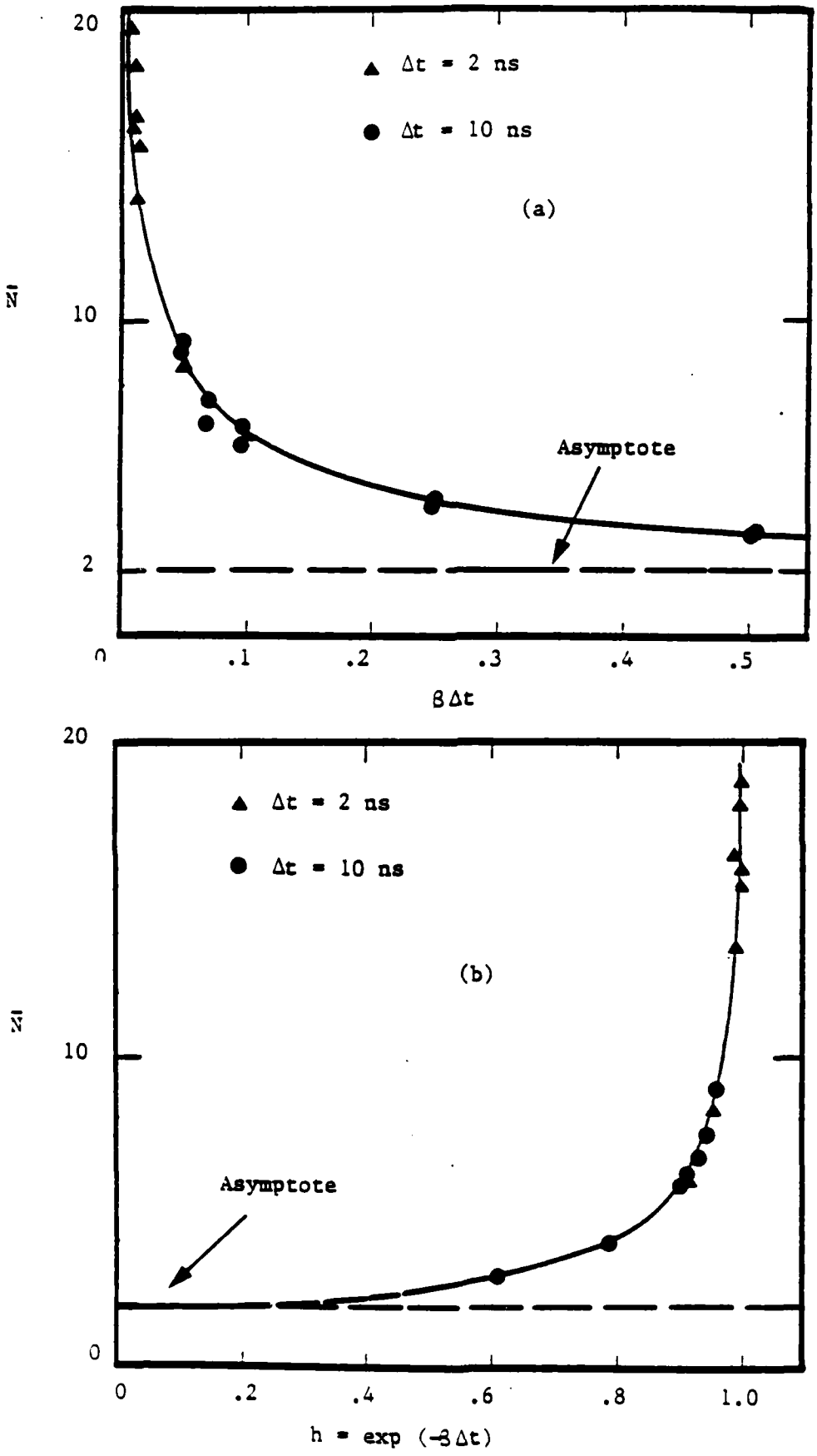

Figure 4.5. Monte Carlo Simulation Result of the Mean Time Step ($\bar{N}$) Between Zero-Crossings of the Velocity, (a) as a Function of $\beta\Delta t$; (b) as a Function of $h = e^{-\beta\Delta t}$.

therefore the values of β, which would lead to the values for ξ/m), it is necessary to have a time resolution of Δt such that $\beta\Delta t \ll 1$ (or $h = e^{-\beta\Delta t}$ close to 1).

4.3 Summary

A theoretical analysis of the probability of obtaining a time τ between consecutive zero-crossings of the Brownian velocity u has been presented. Since u is a random variable, the probability $P(\tau)$ is necessarily a function of the integration time Δt of the instrument used to observe u. The analysis has been carried out in terms of discretizing the time in steps of Δt, $t_n = n\Delta t$, and the resulting probability P(N), $(N = \tau/\Delta t)$, has been derived. The values of P(N) are found to be dependent on the "memory" h ($h \equiv \exp(-\beta\Delta t)$) of the Brownian velocity, where β^{-1} is the relaxation time. For very short memory ($h \ll 1$), the probability P(N) tends to the binomial limit $P(N) = 1/2^N$. The expectation value $\bar{N}$ ($\equiv \sum NP(N)$ assumes the value of 2 in the binomial limit and $2 + O(h^2)$ for small h. For large relaxation time ($\beta \to 0$), $\bar{N} \to \infty$. To obtain accurate information from the measurement of $\bar{N}$ about h, and therefore, the value of β which is related to the physical properties of the particle suspended in the fluid, it is necessary to have $\beta\Delta t < 1$. Since the result is a function of the integration time Δt, which is not a precisely defined quantity for the measuring instrument, the Brownian motion sensor must be a calibrated instrument.

4.4 References for Chapter 4

1. Chandrascklar, S., "Stochastic Problems in Physics and Astronomy," Reviews of Modern Physics, Vol. 15, 1, 1943.

2. Rice, S.O., "Mathematical Analysis of Random Noise," Bell System Technical Journal, Vol. 23 and 24.

5. LABORATORY EXPERIMENT FOR BROWNIAN MOTION DETECTION

In this chapter, the signal to noise requirement for detecting the Brownian motion of a small particle using an interferometric system is first estimated. Then the experimental set up and the data acquisition systems are described. Finally, the signal sampled from the detection system is presented.

5.1 Signal to Noise Requirement of Brownian Motion Detection

The signal from the photomultiplier has a noise component due to the random arrival of the photo-electrons (shot noise), a deterministic frequency component due to the convection of the particle through the fringed volume formed by the intersecting laser beams (regular Doppler signal), and a statistical component due to the Brownian motion of the particle. Since the displacement of the particle due to Brownian motion is small compared to the fringe spacing (see Chapter 2), all the information that can be obtained from the signal on the Brownian motion characteristics is contained in the small fluctuation which is superimposed on top of the regular Doppler signal. To be able to detect this information, the signal fluctuation due to Brownian motion must be much larger than that due to shot noise within the bandwidth of the detector.

The bandwidth Δf of the detector should be able to resolve the relaxation time τ_{relax} of the particle. For particles 0.02 to 0.2 μm in diameter, $\tau_{relax} \sim 3 \times 10^{-8}$ to 3×10^{-7} s. Therefore Δf is $\gtrsim 3 \times 10^{7}$ Hz. The shot noise current is

$$i_{sn} = \sqrt{(2ei\Delta f)} \tag{5.1}$$

For a heterodyne system, the statistics limited signal to noise ratio is

$$S/N = \sqrt{\dot{n} \sin (2\pi x_m/\lambda_f)/\Delta f} \tag{5.2}$$

where $\dot{n}$ is the number of photo-electrons collected per unit time and Δf is the bandwidth. The sine factor is due to the fact that the excursion of the particle due to Brownian motion is small compared to the fringe spacing λ_f, hence the modulation of the heterodyned signal is not complete, and the modulation depth is proportional to the maximum excursion distance X_m occurring during τ_{relax}. Furthermore, the bandwidth should be fast enough to capture τ_{relax} for the smallest particle of interest. The relaxation time for a 0.02 μm particle is 4×10^{-8} s. Therefore a bandwidth of 25 MHz is sufficient. The data acquisition system to be described has a bandwidth of 30 MHz, and this figure is used for the signal to noise calculation. (Note that to resolve t_{relax}, the sampling rate should be at least twice the bandwidth according to the Nyquist theorem. In our data acquisition system, the sampling rate was 100 MHz).

In terms of the parameters of the optical system, the signal to noise ratio for a collection optical system oriented at a 90° scattering angle may be expressed as

$$S/N = \sqrt{\left(\frac{I\tau_r}{A_L}\right)\eta \, d\Omega \left(\frac{d\sigma}{d\Omega}\right)_{90°} \frac{\sin(2\pi x_m/\lambda_f)}{\Delta f}} \tag{5.3}$$

where I is the incident beam power (photon/sec), A_L is beam cross section area, τ_r is the collection optics efficiency, η is the quantum efficiency, $d\Omega$ is the collection solid angle, and $d\sigma/d\Omega$ is the differential scattering cross section. For Rayleigh scattering

$$S/N = \left(\frac{d}{\lambda}\right)^3 \left(\frac{2\pi}{\lambda}\right)^2 \left|\frac{n^2-1}{n^2+2}\right| \sqrt{\left(\frac{I_L \tau_r}{A_L}\right) \eta d\Omega \frac{\sin(2\pi x_m/\lambda_p)}{\Delta f}} \tag{5.4}$$

The d^3 size dependence is due to the variation of the Rayleigh scattering cross section ($\sim d^6$).

For particles in the 0.02 to 0.2 μm range, Eq. (5.5), which is based on Rayleigh scattering, is not strictly valid. Comparisons with the exact Mie calculations at 0.2 μm for a laser wavelength of 0.5 μm, however, showed that the scattering amplitudes calculated by the Rayleigh formula are less than 30% off. For an order of magnitude S/N estimate in the 0.02 to 0.2 μm range, therefore, Eq. (5.5) is sufficient. The signal to noise ratios for systems with laser power density of 10^{10} W/m^2 and 10^9 W/m^2 for each of the intersecting beams, and with f/1.3 collecting optics, $\tau_r = 0.3$ and $\eta = 0.2$ are shown in Figure 5.1. The refractive indexes used in the calculations were 1.5 + 0i, which corresponds to that of latex spheres, and 4.5 - 1.9 i, which corresponds to solid carbon particles. (The latter value is used as a simulation for the S/N in soot measurements.)

For measurements on latex particle used as a calibration procedure, the estimated signal to noise is marginal, ~1 to 10, even for particles up to 0.2 μm. The actual S/N attainable, therefore, is very much dependent on the actual apparatus.

5.2 Apparatus Development

The observation of the Brownian motion of individual small particles poses several experimental design challenges due to the small scattering cross section of the submicron particles combined with the short observation time required to resolve the Brownian motion. As a result, the experiment was severely limited by signal to noise considerations, and much effort focused on refining the optical system to improve the signal to noise ratio. Several versions of the apparatus were developed in an evolutionary manner.

The optical system which had been first assembled for this study is shown schematically in Figure 5.2. A Spectra-Physics Model 165 argon ion laser with a nominal single-line power of approximately 2.5 W which yields a true

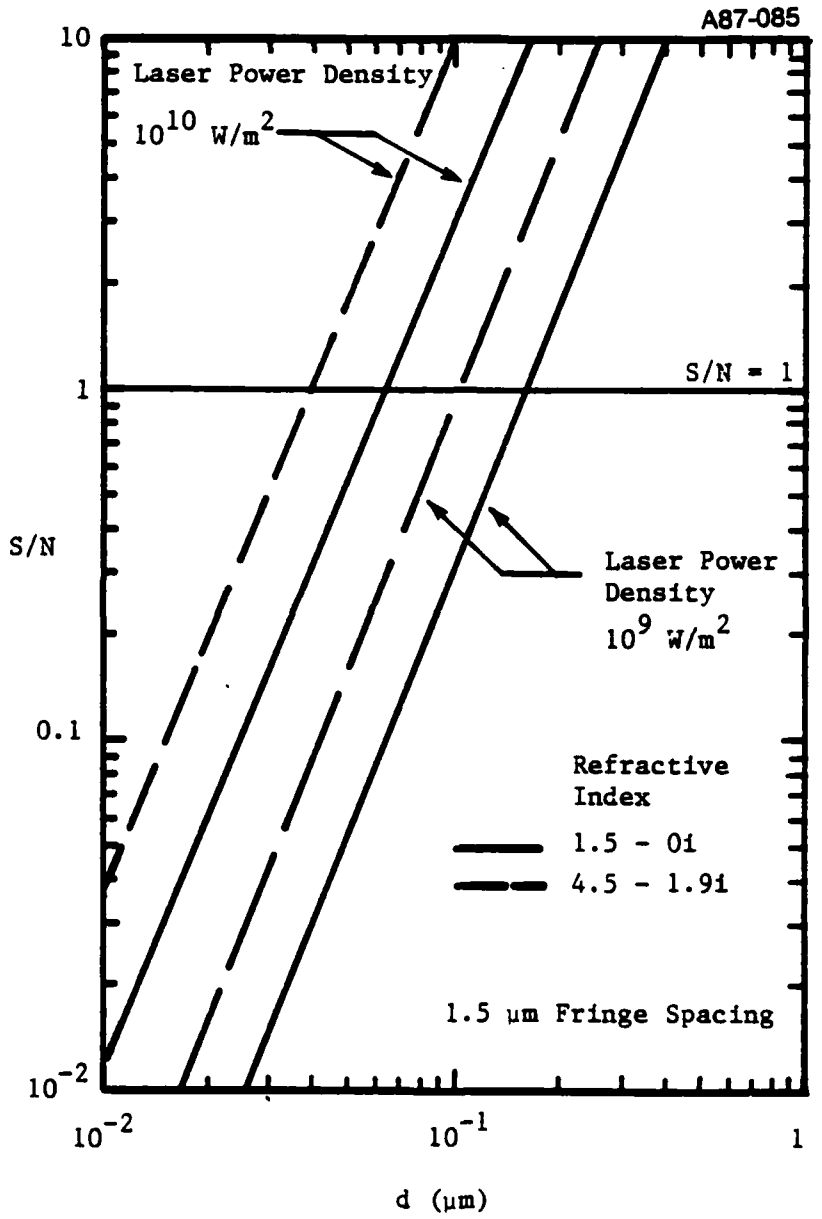

Figure 5.1. Estimated Signal to Noise Ratio of Brownian Motion Detection System. (The calculation is not valid for $d > 0.2$ μm because the Rayleigh scattering formula was used for the scattering cross-section.)

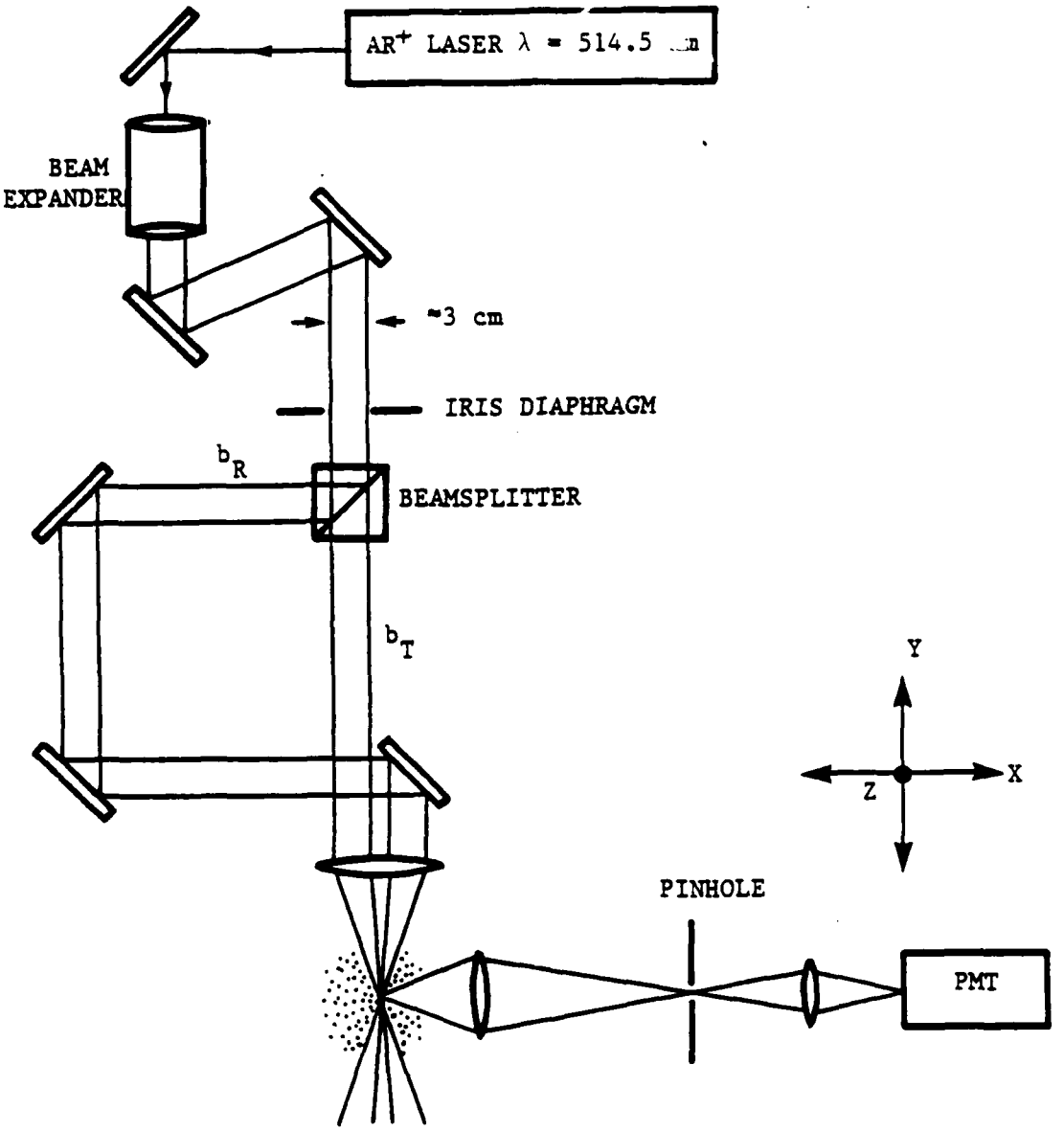

Figure 5.2. Schematic of Experimental Optical System for the Study of Brownian Motion of Individual Submicron Particles.

TEM_{00} output with optimum focusing characteristics was used. To obtain a clear fringe pattern at the measurement volume, it was necessary to insert a Spectra-Physics Model 589 air spaced etalon into the laser cavity to restrict laser oscillation to a single longitudinal mode. This provided the stable mode amplitude and increased coherence length required in our optical measurement system, but at the expense of a 75% decrease in laser power. The vertically polarized output of the laser was expanded by 25x and collimated to a beam size of approximately 3 cm. The beam expansion lead to tighter focusing and a resultant higher power density at the sample volume than could be achieved with a smaller diameter beam. An adjustable iris diaphragm was used after the beam expander/collimator to select the beam diameter.

The expanded beam was split into two beams (b_R and b_T) by a 50/50 cube beamsplitter, which reflected 50% of the incident light and transmited 35%. An increasing intensity difference in two beams when focused to a point to form interference fringes resulted in a decreasing clarity of the fringe pattern, which was detrimental to the signal to noise ratio in our optical system. Therefore, three reflectors were used to decrease the intensity of the reflected beam ($\approx$ 10% light loss off of each mirror) as well as to position this beam on a path parallel to the transmitted beam (b_T). The two beams of approximately equal intensity were then focused by a multi-element lens with a 17.4 cm focal length to form an interference fringe pattern at the sample volume. The sample volume was imaged through a pinhole and then refocused onto a fast photomultiplier (Type R663) which views the light scattered at 90°. An interference filter was used before the photomultiplier to reject light outside a 1 nm band centered at 514.5 nm.

The measurement volume is defined by the intersection of the laser beam intensity profile and the field of view provided by the pinhole of the receiving optics. Its geometry is depicted in Figure 5.3. The incident beams were at a 7.5° angle with respect to each other and had a total power of 130 milliwatts with the iris diaphragm fully open. The fringe pattern formed from the two beams was easily viewed by magnifying the measurement volume by a

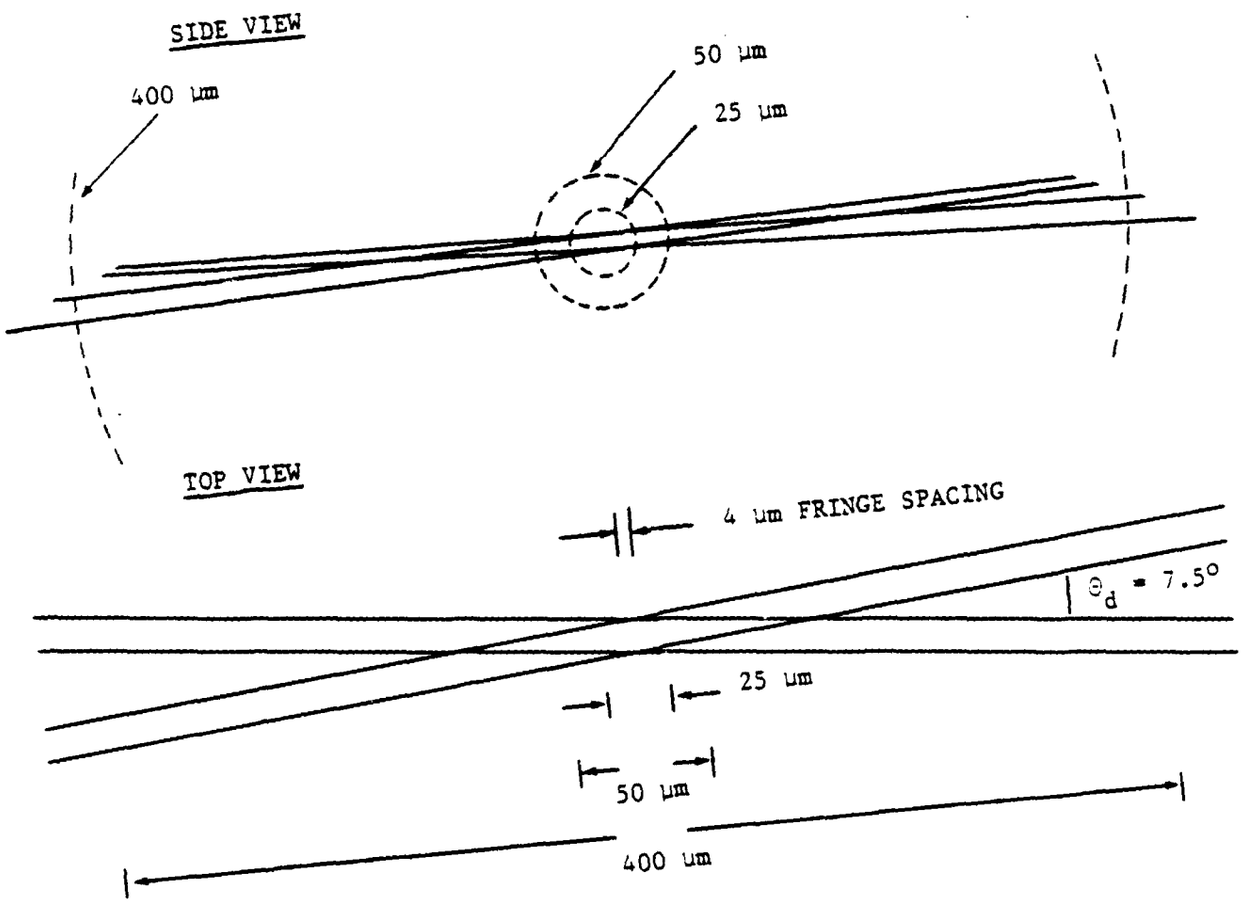

Figure 5.3. Geometry of the Sample Volume, as Seen With the Field of View of 25, 50, and 400 µm Pinholes.

factor of 200 with a microscope lens and projecting it onto a screen. The number of observed fringes is consistent with a calculated 4 μm fringe spacing and 12 μm beam diameter (Figure 5.4).

A successful measurement requires the double coincidence that a single particle traverse the fringe system and be detected within the field of view of the receiving optics. Initially, the measurement volume was imaged onto a 25 μm pinhole with a magnification of unity, but low counting rates were observed with such a small field of view. Also, the detection of scattered light through the small pinhole was highly susceptible to random mechanical vibrations. A 400 μm pinhole was subsequently used and the signal detectability was greatly increased, however, the measurement volume was too large. Extraneous signals from the interaction of a single beam with a particle arose because the field of view of 400 μm was not restricted to the overlap region of the two beams. Also, the larger field of view increases the chance of detecting multiple particle events. Finally, the sample volume was imaged with a magnification of ≈ 10 onto a 400 μm pinhole. This was equivalent to a field of view of 40 μm and rendered the signal less susceptible to vibrations. The collection optics consisted of a 60 mm diameter 70 mm focal length plano-convex lens located ~77 mm from the measurement volume. The overall optics have a f number of ~1.3.

5.3 Signal Acquisition System

The data acquisition system is shown in Figure 5.5. The signal from the photomultiplier tube was amplified by a high speed buffer amplifier (200 MHz bandwidth, x100 gain). The Brownian motion data was recorded on a Data Precision Flash A/D system with high speed memory. For each event (traversal of a particle through the probe volume), 8192 data points at 10 ns interval were collected. The record length of 8 μs of data was large compared to the relaxation time of the particle which is of the order of 0.1 μs; therefore there should be enough data for statistical analysis.

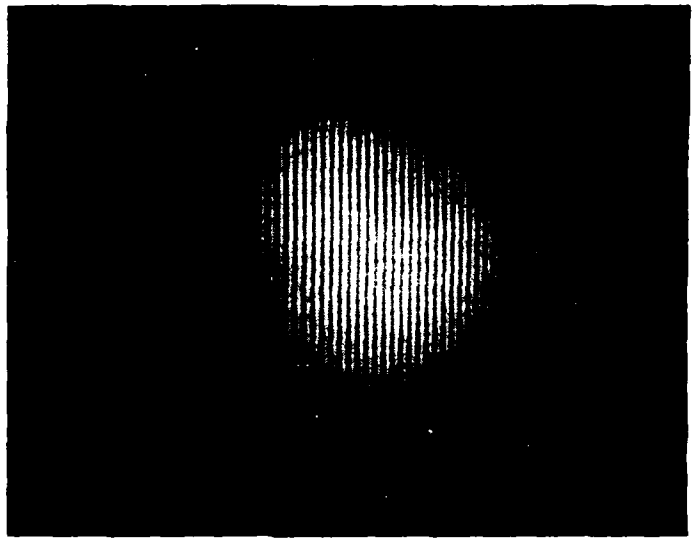

(a)

(b)

Figure 5.4. Magnified View of the Interference Pattern: (a) With a Narrow Unfocussed Beam Diameter (~0.2 μm Beam Diameter); (b) With a 2.2 cm Unfocused Beam Diameter. The weak interference fringes in the background of (b) are due to scattered light from the microscopic objective.

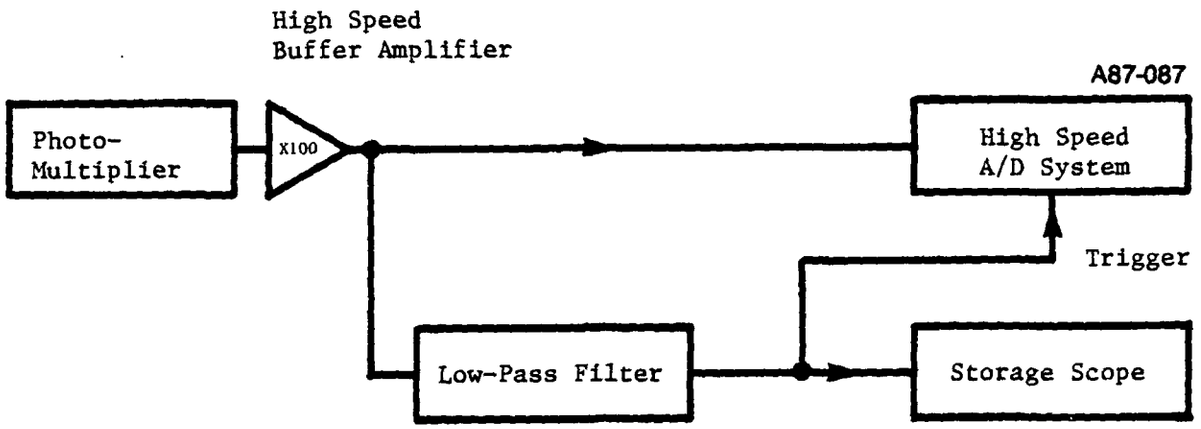

Figure 5.5 Schematic of Data Acquisition System

To verify that the Brownian motion signal was captured when the particle was located at the "steep" part of the fringe pattern, the signal from the buffer amplifier was fed through a low pass filter to provide the trigger signal for the data acquisition system. The filter frequency was set at approximately the Doppler frequency due to the convection velocity of the particle through the measurement volume. A typical trace of the filtered signal which was recorded by a storage oscilloscope simultaneously with the high speed Brownian motion data is shown in Figure 5.6. Because the trigger level was known, the portion of the signal captured by the high speed data acquisition system may be identified on the scope trace as in Figure 5.6. If this portion of the signal was not located at the "steep" part of the fringe pattern (as shown), the particular data record was discarded.

The high speed data record corresponding to the event of Figure 5.6 is shown in Figure 5.7. The top trace in Figure 5.7 is the actual signal sample at 10 ns intervals. The bottom trace is the same signal with the points connected by a (sin x)/x fitting. Stored data records similar to this were used for the statistical analysis.

5.4 Results and Discussion

It was realized that in the initial setup the signal to noise ratio was too small for detection of Brownian motion. The incident beam intensity of 65 mW focused into a 12 μm spot (intensity of 5×10^8 W/m^2) was too low. The system, nevertheless, was set up to verify that the data acquisition system was operational and to assess the actual S/N ratio to determine the improvements necessary to obtain a useful signal. The typical signal records collected were depicted in Figures 5.6 and 5.7. These records were processed digitally for statistical analysis.

To verify the operation, the system was used to look at small latex spheres suspended in water. Since the viscosity of water is $\sim 3 \times 10^3$ times that of air, the signal due to Brownian motion was negligible and the response

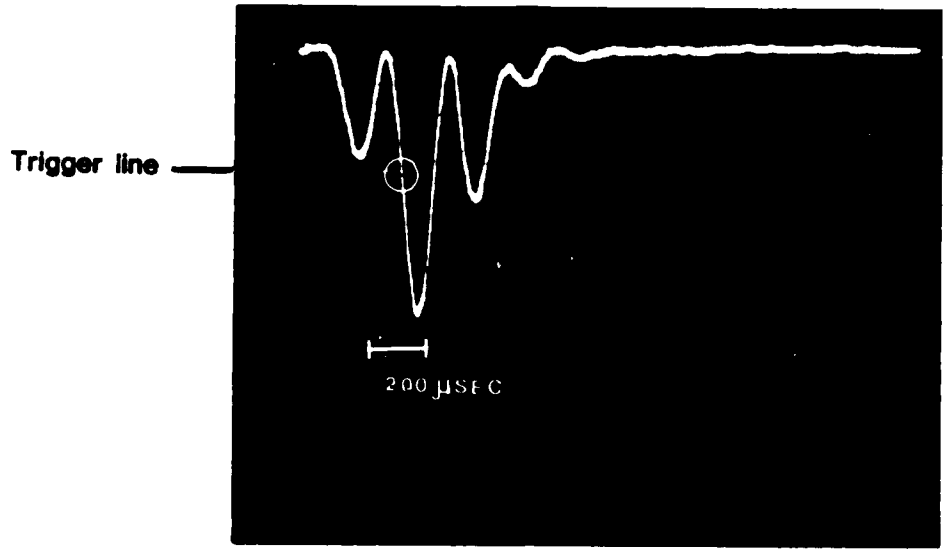

Figure 5.6. The Filtered Signal From the PMT. The signal was used to trigger the 100 MHz data acquisition system. The portion of signal recorded is marked by the circle (8,192 samples at 10 ns sampling intervals).

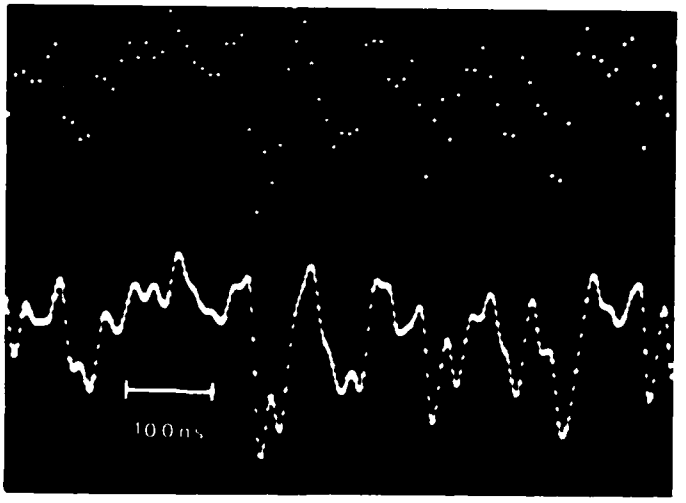

Figure 5.7. Signal Recorded by the Fast A/D System. (a) Actual Signal Sample Points at 10 ns Sampling Intervals. (b) Sample points connected by sin x/x fit.

of the system was mainly due to shot noise. Therefore, the measurement established the noise limit of the system. The signal was processed to obtain histograms of the time between extrema of the signal as described in Chapter 3. The histograms for particles of several sizes are shown in Figure 5.8, which shows that there was no difference in signal response for different size particles. This is because the signal was masked by the shot noise. (The peak at 30 ns is probably due to the 30 MHz bandwidth of the system.)

To improve the signal to noise ratio of the system, two changes were made. The receiving optics were rearranged to a forward scattering collection geometry, and the focusing lens for the incident beam was replaced by one with a shorter focal length (7 cm compared to 17.4 cm). The 2 cm diameter incident beams were focused to a ~4 μm spot. The fringe spacing was 1.5 μm and there were 3 fringes in the focal volume. The change of the focusing lens improved the signal by increasing the beam intensity and decreasing the fringe spacing. The intensity of each beam at the measurement volume was ~5 x 10^9 W/m^2.

The above system was tested by injecting latex particles of 0.045, 0.087 and 0.261 μm diameters through the measurement volume. These particles were commercially available as concentrated aqueous suspension in small vials. The suspension was diluted with alcohol and dispersed with an air nebulizer. The concentration of the suspension was such that it was unlikely to have more than one particle in each nebulized droplet. The droplets were mixed with a stream of drying air to remove the liquid content to ensure that dry latex particles were introduced into the measurement volume.

The signal to noise ratio was calculated from the measured photocurrent and the known gain of the photomultiplier. For the particles used, the photo-electron arrival rate was estimated to be $\dot{n} = 10^{10}/s$. The Brownian excursion x_m for these particles is approximately 1 percent of the wavelength λ. Therefore, for a 30 MHz bandwidth system, the signal to noise ratio according to Eq. (5.2) was ~5. Because the signal processing strategy

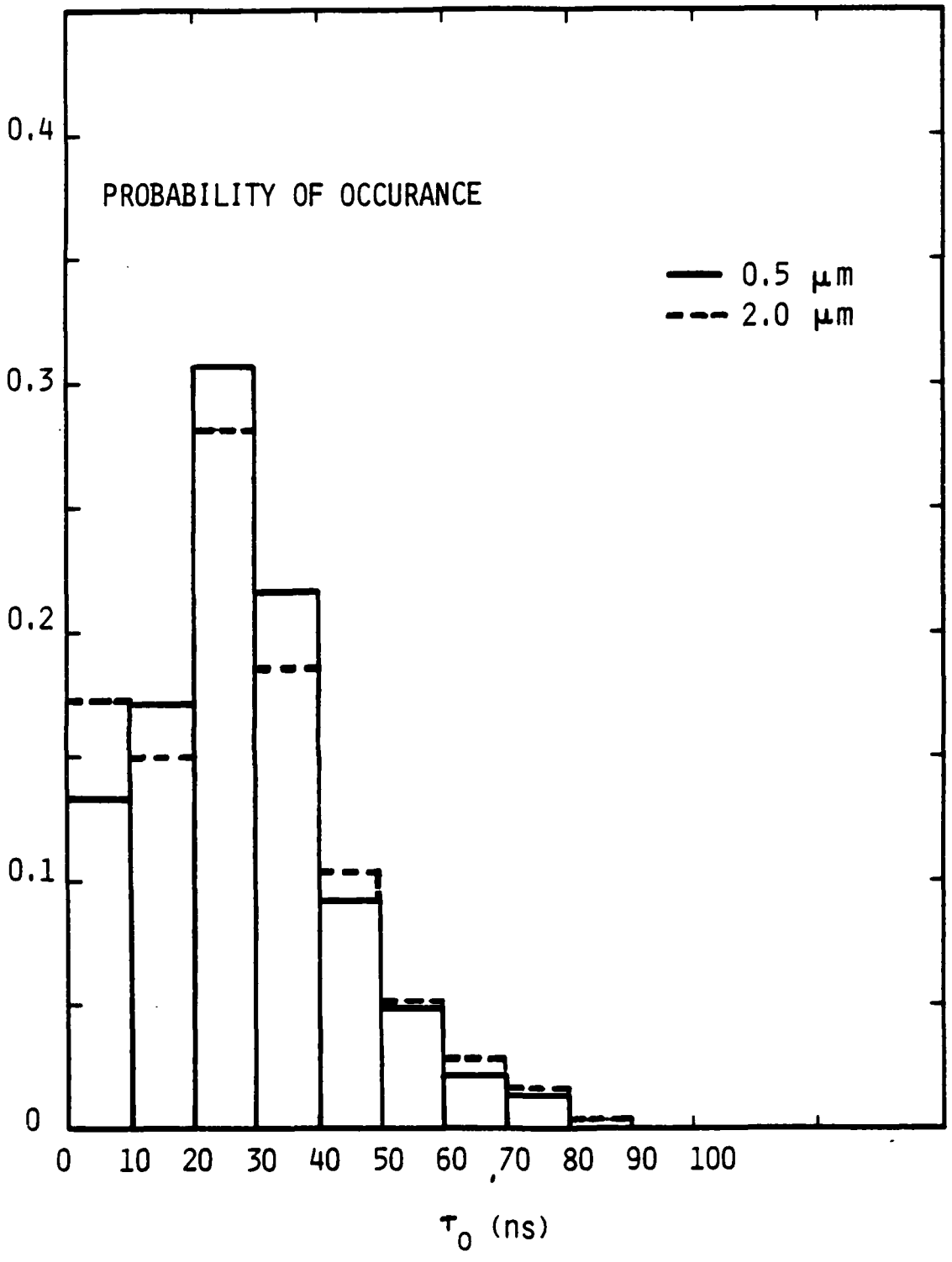

Figure 5.8. Histogram of the Time Between Extrema of the Doppler Signal From Latex Spheres Suspended in Water.

relied on the frequency modulation (the time between extrema) to recover the necessary information, it was especially susceptible to noise. A signal to noise ratio of 10 is the minimum acceptable value. Therefore an increase of S/N by at least a factor of 2, or signal level a factor of 4 is necessary.

The optical system had been designed, approximately, to the limitation of commercially available optical components. The intensity gradient at the focal volume had been maximized for a given laser power. The single mode, etalon stabilized laser power, however, may be easily increased by using a newer model laser. Alternatively, the instrument may be used to look at particles in the $> 0.2\ \mu m$ range (the S/N is proportional to d^6). At a higher beam intensity, however, other physical processes begin to play an important role in modifying the Brownian motion behavior. These processes and the limitations imposed by them are discussed in the next chapter.

6. DETECTION LIMIT OF BROWNIAN MOTION

The scattered light from a particle may be increased by increasing the intensity of the probe laser beam. There is a limit, however, on the maximum beam intensity because it will disturb the dynamics of the particle Brownian motion. There are two effects: (a) the particle may be heated so that the thermal environment changes, and there is a substantial thermophoretic effect. (We are not considering the severely heated case in which the particle may vaporize or ignite.) (b) At high beam intensity, the photon pressure may change the dynamics of the particle motion. The thermophoretic effect depends on the particle absorptivity and the thermal properties of the particle and the fluid. The photon pressure effect is present independent of the particle absorptivity. These effects determine the limit of detection of the Brownian motion. In the following, the above effects will be examined. The particles are assumed spherical and the diameters of interest are in the range of 0.02 μm to 0.2 μm. A diameter of 0.1 μm is used as the nominal value to estimate the effects quantitatively. The laser beam power P is assumed to be 1W at 0.5 μm wavelength and is focused into a spot of diameter b ~10 μm. The beam intensity is $\sim 10^{10}$ W/m^2. These values would correspond to a 1 cm diameter beam focused to a spot by a 10 cm focal length convex lens. The thermal environment of the particle is atmospheric air at 300 K. The particles are assumed to be convected through the probe volume at a velocity U ~10 cm/s.

Since the mean free paths Λ of the air molecules at atmosphere is ~0.06 μm, particles in the range of 0.02 to 0.2 μm are in the transition flow regime (Knudsen number $k_n = \Lambda/d$ ~3 to 0.3). The theory of transition flow has not been well established. The present calculations were based on an empirical fit to the available data.[6.1,6.2]

6.1 Thermal Characteristics of the Particles

In the flow regime considered here, heat transfer from the submicron particles by forced convection and natural convection are negligible due to the extremely small Reynolds number and Grashof number. The major heat removal mechanism is through conduction. Data on the heat transfer from a sphere in a rarefied gas from Ref. [6.2] may be fitted as:

$$\frac{N_u}{N_{uc}} = 1 - \exp\left(\frac{0.215}{k_n} + \frac{0.0275}{k_n^2} - \frac{2.815 \times 10^{-3}}{k_n^3} + \frac{1.346 \times 10^{-4}}{k_n^4} - \frac{2.295 \times 10^{-6}}{k_n^5}\right) \quad (6.1)$$

where the Nusselt number (N_u) is evaluated at the free stream properties and N_{uc} is the Nusselt number at the continuum limit ($N_{uc} = 2$). With a 0.1 μm diameter particle in atmospheric condition, $N_u \sim 0.5$. Values for N_u as a function of k_n are shown in Figure (6.1).

As the particle enters the beam volume, it is heated up by the laser beam because of the finite absorptivity. The heat up time may be estimated by considering the thermal diffusion time through the particle as well as the boundary layer. For an order of magnitude estimate, we used the properties of polyethylene particles with a thermal diffusivity $\alpha_p \sim 8 \times 10^{-8}$ m^2/s. The temperature distribution inside the particle will become steady state in $t_p \sim d^2/\alpha_p$. For particles in the 0.02 to 0.2 μm range, $t_p \sim 0.005$ to 0.5 μs. The thermal diffusion time through the boundary layer may be obtained from the energy balance on the particle

$$m\, c_p \frac{dT}{dt} = Ia \frac{\pi d^2}{4} - N_u\, \pi d^2\, k(T-T_\infty)/d \quad (6.2)$$

where m, c_p are the mass and specific heat of the particle, I is the laser beam intensity, a the absorptivity of the particle, and k the thermal conductivity of the air. The thermal diffusion time from Eq. (6.2) is therefore:

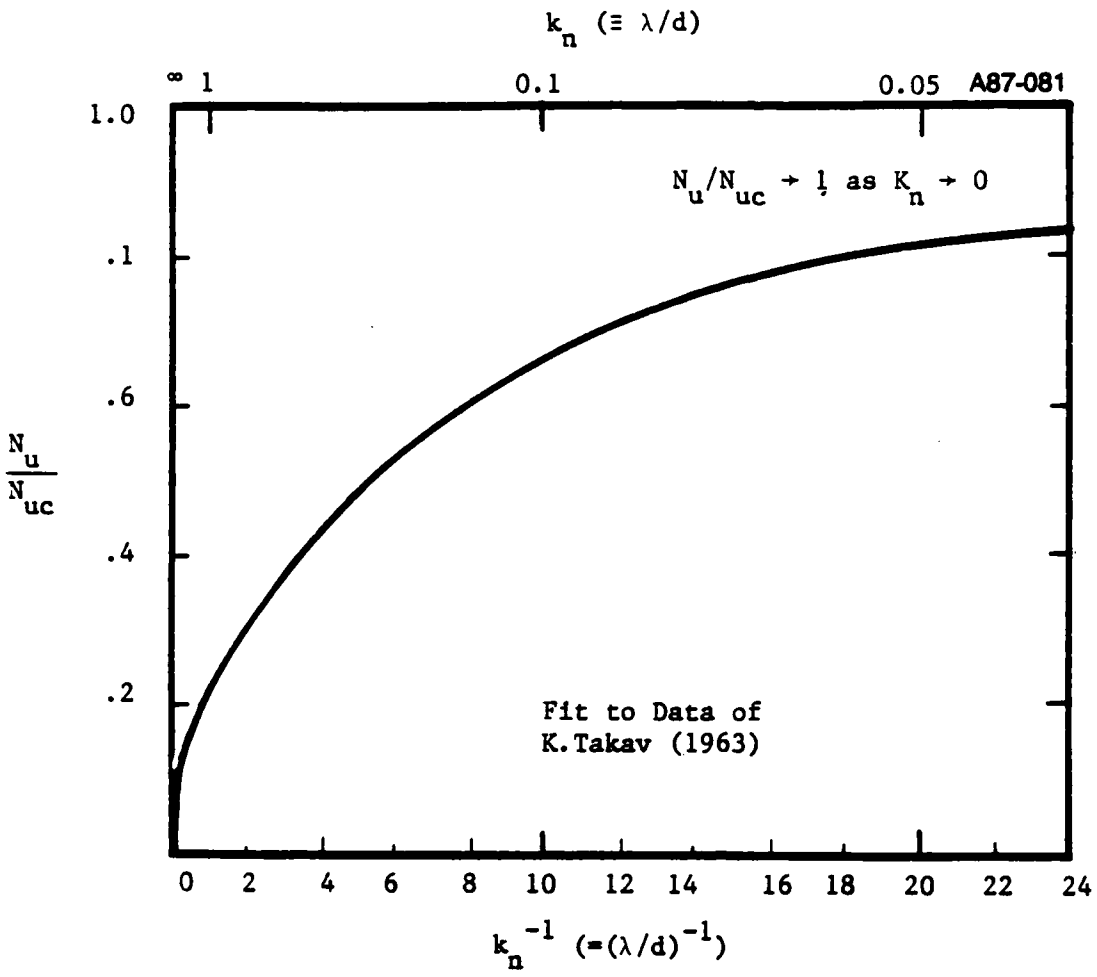

Figure 6.1. Heat Transfer Characteristics of a Sphere in a Rarefied gas; data from Ref. 6.2.

$$t_a = \frac{1}{6\ N_u} \left(\frac{d^2}{\alpha_p}\right) \left(\frac{k_p}{k}\right) \tag{6.3}$$

where k_p is the thermal conductivity of the particle. For polystyrene particles, (k_p/k ~5.5) the thermal diffusion time, t_a, through the particle in the 0.02 to 0.2 μm size range is, therefore, ~0.04 to 0.6 μs.

Since the particle residence time t_s = b/u is of the order of 100 μs, which is much longer than t_a and t_p, the temperature distribution both inside and around the particle may be considered at steady state for the following analysis.

The steady state temperature rise is plotted against the product Ia in Figure 6.2 for particles in the 0.02 to 0.2 μm range. To avoid a substantial perturbation of the thermal environment, Ia should be less than 10^7 W/m^2. For the 1W beam focused to 10 μm square beam spot (I ~10^{10} W/m^2), the particle absorptivity should be 10^{-3} or less. Thus the method cannot be used for particles such as soot particles which have a high absorptivity.

6.2 Thermophoresis of the Particles

When a particle with non-zero absorptivity is illuminated by a laser beam, thermophoresis occurs because a temperature gradient is set up so that the illuminated side of the particle has a higher temperature than the shadow side. The net result is that the particle acquires a drift velocity in the laser beam direction. This problem may be studied in a similar manner to the classical analysis[6.3] of thermophoresis of small particles in thermal equilibrium with a gas in which a temperature gradient is present. In the present case, however, the boundary condition on the particle surface would have to be modified to include the heat flux due to the absorption of the laser light, and the temperature field far from the particle would be uniform. Such a case has not been discussed in the literature. To develop the solution for this case would be beyond the scope of this study. We, therefore, use a simple one dimensional energy balance estimate of the temperature gradient across the particle, and then estimate the thermophoretic effect using this temperature gradient and the semi-empirically based formula suggested by Ref. [6.4].

In the one dimensional model of this "spherical" particle, the particle is modelled as a cylinder of diameter d and length d as shown in Figure 6.3. The side wall of the cylinder is assumed to be adiabatic. Each end of the cylinder is fitted with a heat exchanger of area $\pi d^2/2$, representing the surface area of one half the original sphere. The heat transfer characteristics of these heat exchangers are specified through the Nusselt number of a sphere in a rarefied flow. The temperature profile is shown in Figure 6.3. The power input from the laser beam is Ia $\pi d^2/4$. In steady state, therefore,

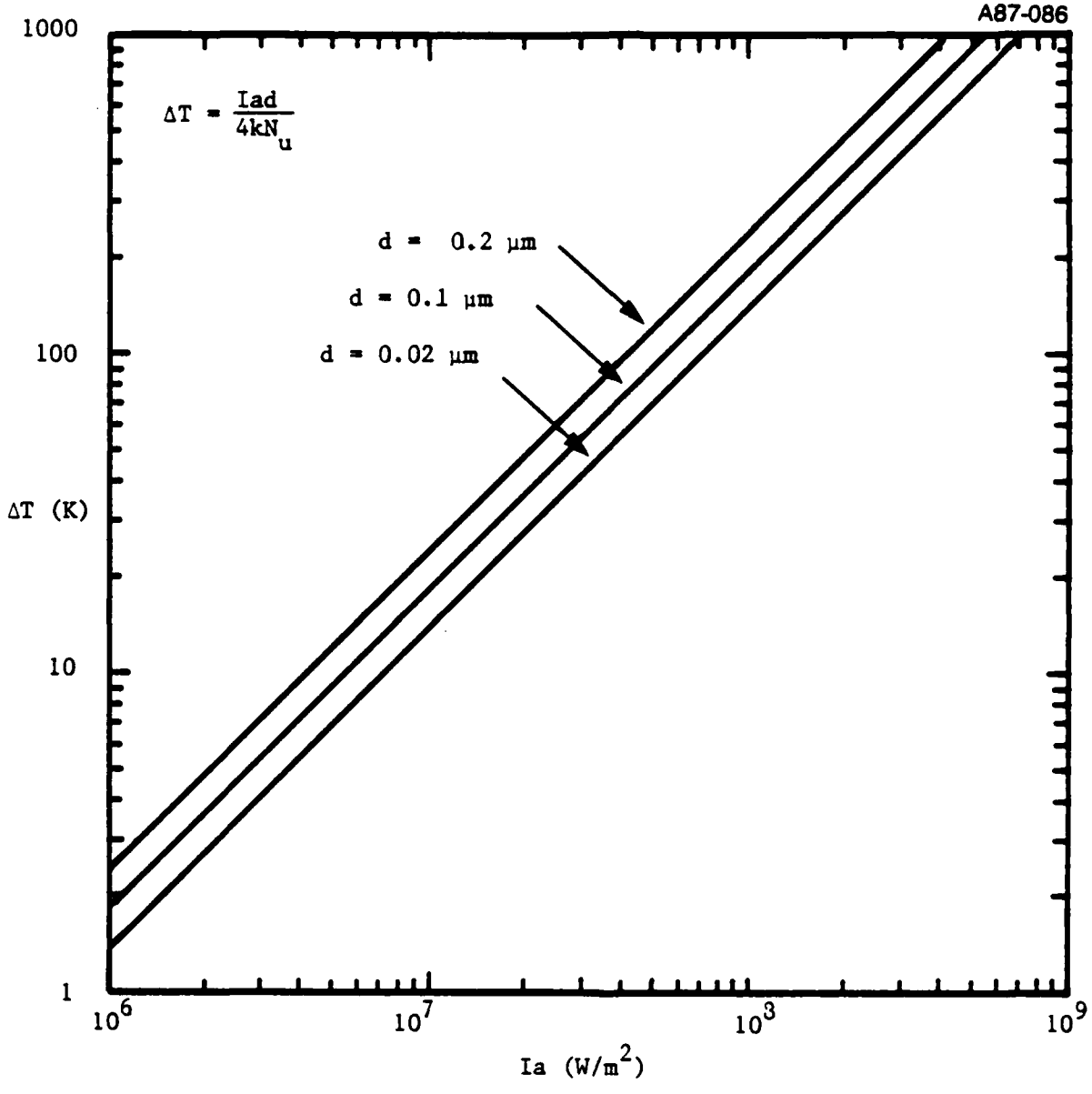

Figure 6.2. Temperature Rise As a Function of the Product of Beam Intensity and Particle Absorptivity

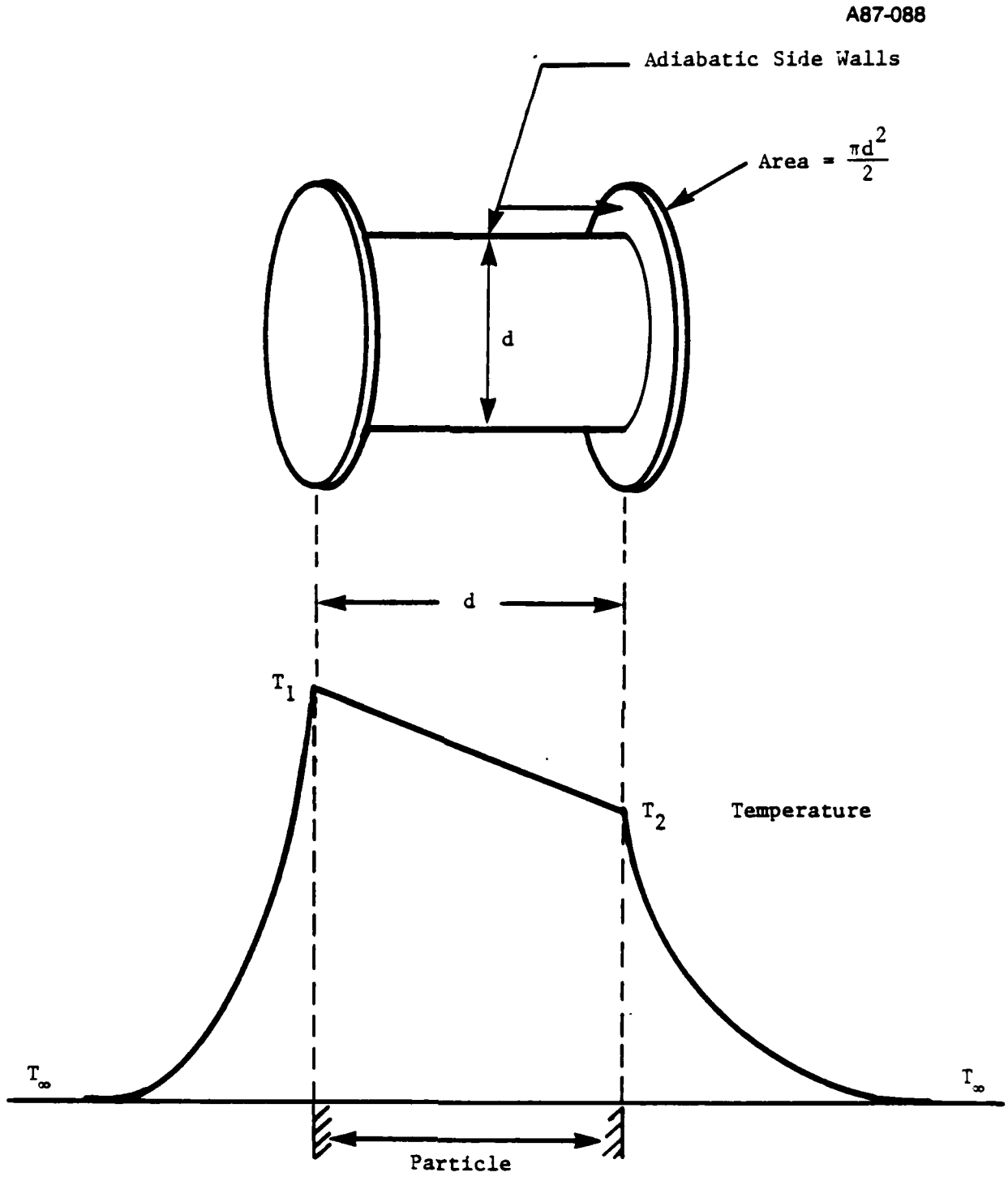

Figure 6.3. One Dimensional Model of a "Spherical" Particle

$$\text{Nu } k \left(\frac{T_1 - T_\infty}{d}\right) \frac{\pi d^2}{2} + \text{Nu } k \left(\frac{T_2 - T_\infty}{d}\right) \frac{\pi d^2}{2} = \text{Ia} \left(\frac{\pi d^2}{4}\right) \tag{6.4}$$

and

$$\text{Ia} \frac{\pi d^2}{4} - \text{Nu } k \left(\frac{T_1 - T_\infty}{d}\right) \frac{\pi d^2}{2} = k_p \left(\frac{T_1 - T_2}{d}\right) \left(\frac{\pi d^2}{4}\right) \tag{6.5}$$

The average temperature $T_{ave} \equiv (T_1 + T_2)/2$ and the temperature difference $\Delta T \equiv T_1 - T_2$ may be calculated from Eq. (6.4) and Eq. (6.5) as

$$T_{ave} - T_\infty = \frac{\text{Ia } d}{4 \text{ Nu } k} \tag{6.6}$$

$$\Delta T = \frac{\text{Ia } d}{2(k_p + \text{Nu } k)} = \frac{2 (T_{ave} - T_\infty)}{[1 + k_p/(k \text{ Nu})]} \tag{6.7}$$

The temperature difference ΔT is plotted in Figure 6.4. It is a significant fraction of the average temperature rise $(T_{ave} - T_\infty)$.

In the near continuum limit, the thermophoretic force F for a particle in equilibrium with a gas in which a temperature gradient is present was calculated by Brock[6.3]

$$F = - \frac{6\pi\mu^2 d \, C_s}{\rho T_0} (\nabla T)_x \frac{(k/k_p + 2 \, C_t \, \Lambda/d)}{(1 + 6 \, C_m \, \Lambda/d)(1 + 2 \, k/k_p + 4 C_t \, \Lambda/d)} \tag{6.8}$$

where C_s (= 1.17) is the thermal slip coefficient, C_t (=2.18) is the temperature jump coefficient, and C_m (=1.14) is the momentum exchange coefficient. Talbot[6.4] argued that this formula is a useful means of interpolation for all values of Λ/d, since it reduces to within 3% of the correct collisionless limit (for perfect accommodation) when $\Lambda/d \to \infty$.

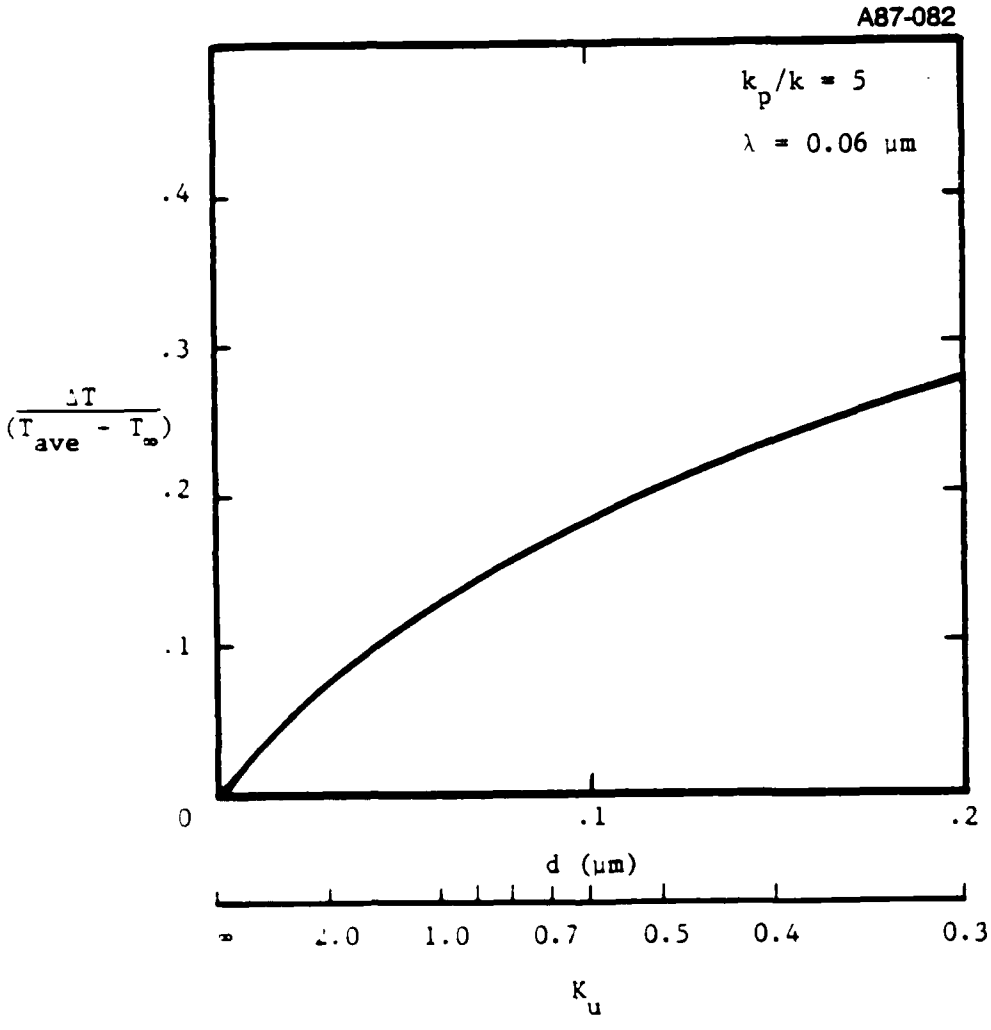

Figure 6.4. Temperature Difference Across a Particle. (k_p and k are the thermoconductivity of the particle and air, respectively.)

Under the action of the thermophoretic force, the particle would attend a terminal velocity in a time scale of the order of the Brownian relaxation time (relax = $\rho_p\ d^2/18\ \mu$). Using the Milliken drag formula,[6.4] the drift velocity is

$$u_T = \frac{2\nu C_s \left(k/k_p + 2C_t\ \Lambda/d\right)\left[1 + \frac{2\Lambda}{d}\left(A + B\ e^{-cd/2\Lambda}\right)\right]}{\left(1 + 6\ C_m\ \Lambda/d\right)\left(1 + 2\ k/k_p + 4\ C_t\Lambda/d\right)} \left(\frac{\nabla T_x}{T_0}\right) \qquad (6.9)$$

where

$A = 1.20$

$B = 0.41$

$C = 0.88$

Although the assumptions leading to Eq. (6.9) do not match the present application, (most importantly, the temperature distribution around the particle would be quite different), a useful estimate of the drift velocity may be obtained by replacing the temperature gradient in Eq. (6.9) with $\Delta T/d$, with ΔT given by Eq. (6.7). If the temperature rise ΔT is not very large, T_∞ may be used for T_0. The thermophoretic drift velocity of the particle and the mean Brownian velocity $\left[\sqrt{(8\ kT/\pi m_p)}\right]$, are plotted against the particle size in Figure 6.5. The thermophoretic velocity u_T is not very sensitive to the particle diameter because ΔT is proportional to d so that $(\nabla T)_x$ is independent of d. At a modest absorbed power density level of 10^7 W/m^2, at which the temperature rise of the particle is ~20°C according to Figure 6.2, the drift velocity is significantly higher than the mean Brownian velocity. Therefore thermophoretic effects could significantly alter the statistics of the Brownian velocity.

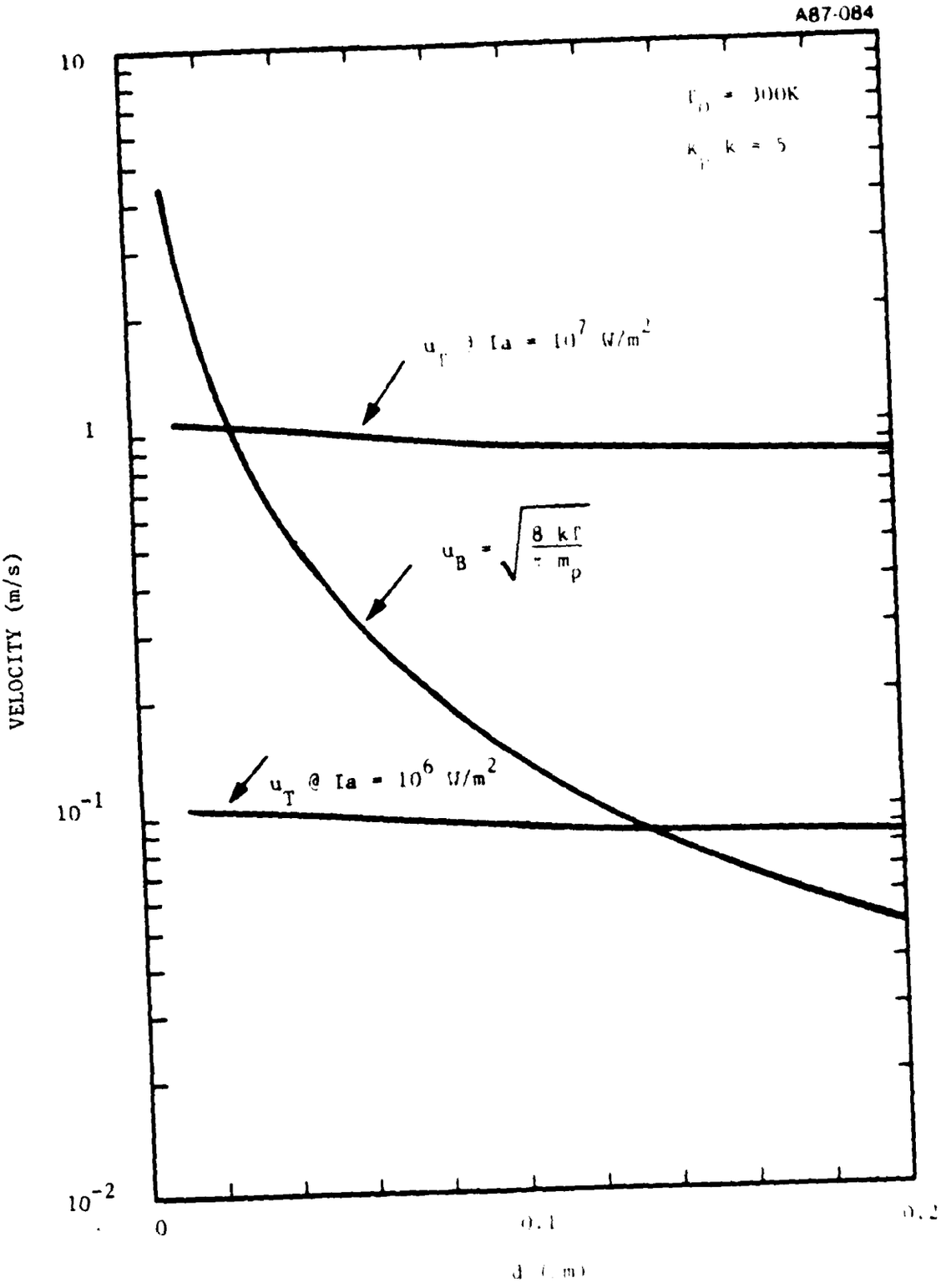

Figure 6.5. Thermophoretic Velocity (u_T) and Brownian Velocity (u_B) of Particles. The laser beam intensity is I, and the particle absorptivity is a.

6.3 Photon Pressure

At high laser beam intensity, there is a significant pressure force on the particle due to the momentum exchange between the photons and the particle. Under the motion of this force, the particle will attend a terminal velocity in a time scale of the order of the Brownian relaxation time ($\tau_{relax} \sim \rho_p\, d^2/18\,\mu$). If the laser beam is uniform and uni-directional, this terminal velocity would not affect the Brownian motion statistics. The actual beam probe volume, however, is obtained by focusing the laser beam to a diffraction limited spot. As a result, both the intensity and direction of the laser light is highly dependent on the position of the particle, and the photon pressure effect is coupled into the Brownian motion. To estimate the effect, we shall calculate the terminal velocity of the particle due to the photon pressure and compare it to the mean Brownian motion velocity.

Consider a particle which is illuminated by a polarized laser beam in the z direction as shown in Figure 6.6. The incident electric field is in the x direction. According to Mie theory,[6.5] the electric field intensity of the scattered light is given by

$$\begin{bmatrix} E_p^1 \\ E_\ell^1 \end{bmatrix} = \begin{bmatrix} \sqrt{i_1(\theta)} & 0 \\ 0 & \sqrt{i_2(\theta)} \end{bmatrix} \begin{bmatrix} E_p^0 \\ E_\ell^0 \end{bmatrix} \tag{6.10}$$

where the scattering amplitudes i_1 and i_2 are in terms of the size parameter $x(=\pi d/\lambda)$ and the refractive index m of the particle. If I_0 is the incident beam intensity (photons/area/time), then the force in the z direction due to the momentum transfer of the scattered photon is

$$F_z = \frac{I_0}{k^2}\frac{h}{\lambda}\int_0^{2\pi} d\phi \int_0^{\pi} d\theta\, \sin\theta\,(1-\cos\theta)\left[i_1(\theta)\sin^2\phi + i_2(\theta)\cos^2\phi\right] \tag{6.11}$$

A87-089

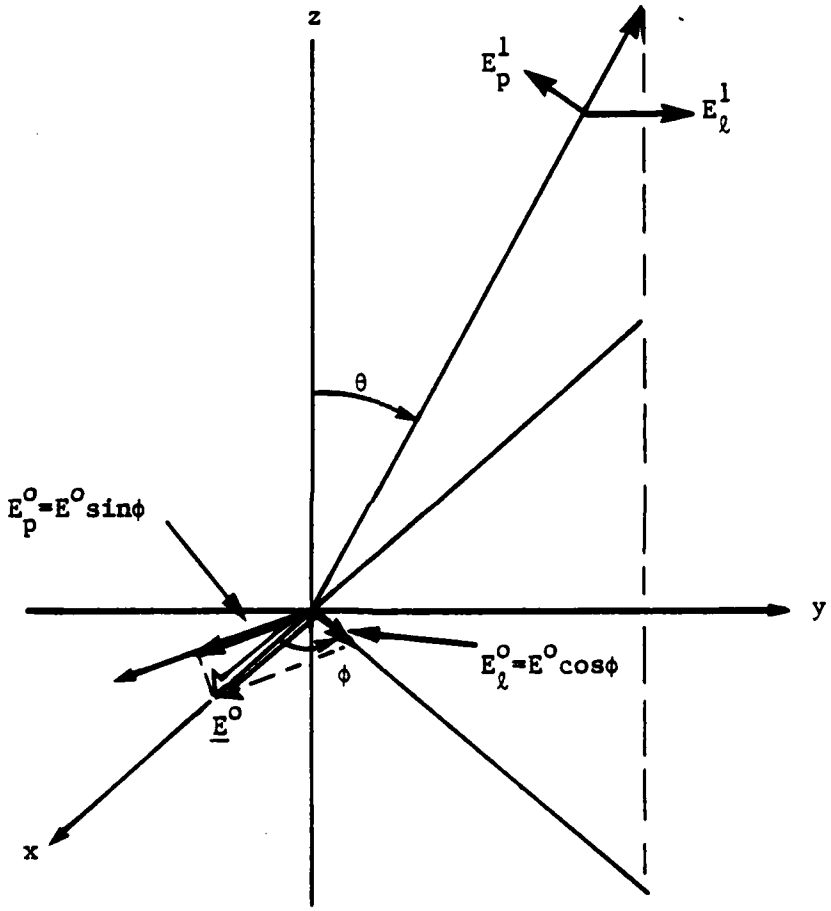

Figure 6.6. Mie Scattering of Particle, Illustrating the Geometry of the Incident and the Scattered Electric Field.

where h is the Planck's constant and the ϕ dependance is illustrated in Figure 6.6. Since $k = 2\pi/\lambda$, and i_1, i_2 are only functions of cos θ, (see Ref. [6.5]), the force due to photon pressure is

$$F_z = \frac{I_0\lambda^2}{(2\pi)^2} \frac{h}{\lambda} \pi \int_{-1}^{1} d(\cos\theta) \left[i_1(\cos\theta) + i_2(\cos\theta)\right] (1-\cos\theta)$$

$$= \frac{I\lambda^2}{4\pi c} \int_{-1}^{1} d(\cos\theta) \left[i_1(\cos\theta) + i_2(\cos\theta)\right] (1-\cos\theta) \qquad (6.12)$$

where I is now the beam intensity in W/m^2. To obtain representative values of F_z, the integral in Eq. (6.12) was evaluated numerically. For a 0.25 μm particle with refractive index m = 1.5 + 0 i, which is representative of the polystyrene test particles, the values for F_z are shown in Figure 6.7. Also shown are the corresponding drift velocities u_D, given by the Milliken formula:

$$u_D = \frac{F_z \left[1 + \left(A + B\, e^{-Cd/2\Lambda}\right) 2\Lambda/d\right]}{3\pi\mu d} \qquad (6.13)$$

The results show that for non-absorbing particles of 0.25μm diameter, the photon-pressure-produced drift velocity is less than the Brownian velocity for beam intensity up to 10^{10} W/m^2. Since the scattering cross section decreases rapidly with particle size, photon pressure would not significantly affect the Brownian motion for beam intensities of $\leq 10^{10}$ W/m^2.

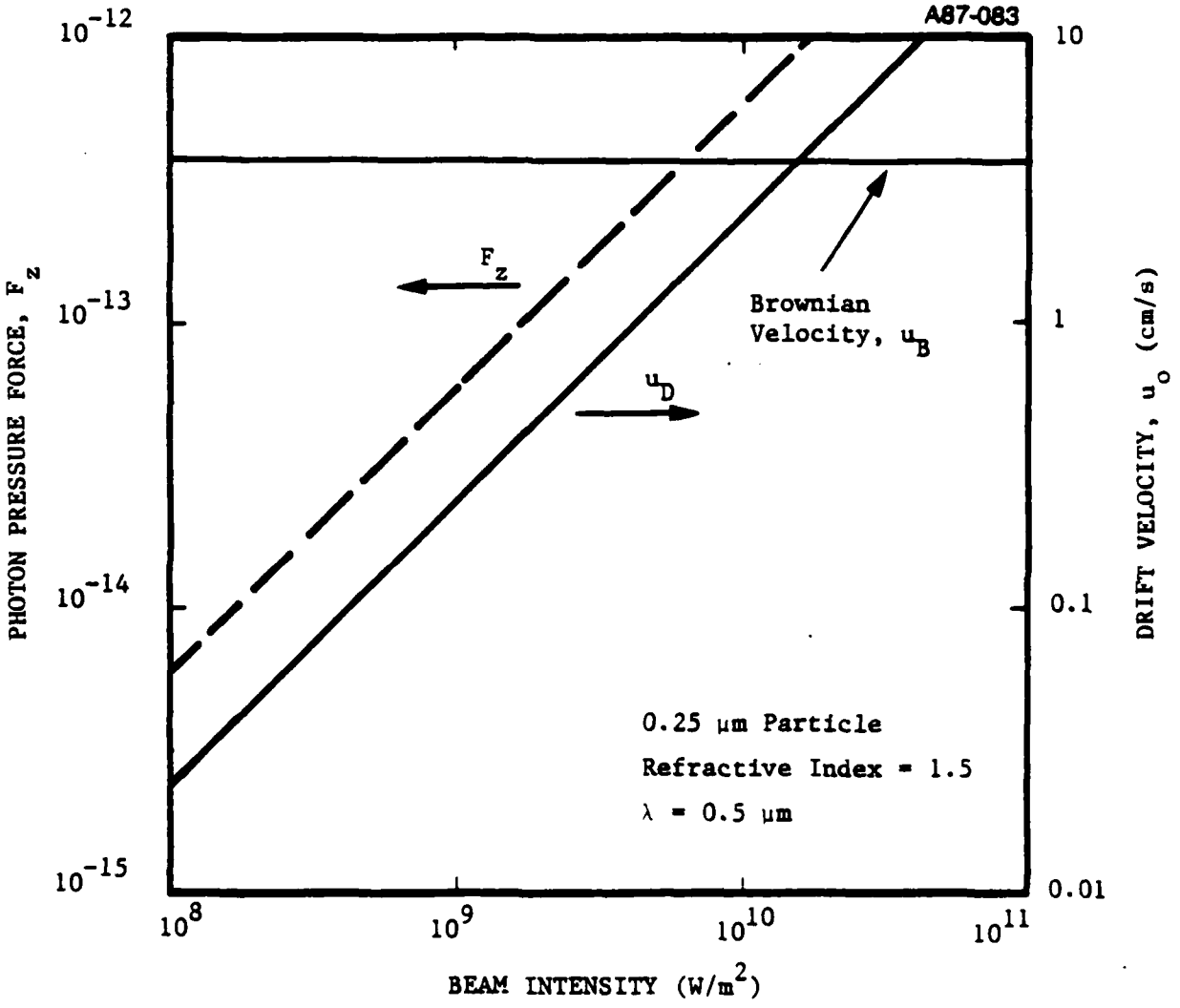

Figure 6.7. Photon Pressure and the Associated Drift Velocity for 0.25 μm Polystyrene Particle

6.4 References for Chapter 6

6.1 F.S. Sherman, "A Survey of Experimental Results and Methods for the Transition Regime of Rarefied Gas Dynamics," Rarefied Gas Dynamics, ed. by J.A. Laurmann, Acad. Press. 1963.

6.2 K. Takav, "Heat Transfer from a Sphere in a Rarefied Gas," Rarefied Gas Dynamics, ed. by J.A. Laurmann, Acad. Press. 1963.

6.3 J.R. Brock, "On the Theory of Thermal Forces Acting on Aerosol Particles," J. of Coll. Sci. 17, 768-780.

6.4 L. Talbot, "Thermophoresis - A Review," Rarefied Gas Dynamics, Progress in Astro. and Aero. 74, ed. by S.S. Fisher, AIAA, 1980.

6.5 H.C. Van De Hulst, Light Scattering by Small Particles, Dover, 1981.

7. SUMMARY AND CONCLUSIONS

A theoretical and experimental study on the feasibility of determining the size of submicron particles by observing their Brownian motion characteristics has been carried out. The motion was detected by using an interferometric system very similar in construction to a conventional laser doppler velocimeter system. The mean excursion associated with the Brownian motion, however, is much smaller than the fringe spacing formed by the intersecting laser beams at the measurement volume so that it is not possible to extract information from the signal using conventional laser doppler velocimeter signal processing. Nevertheless it is possible to determine the damping behavior of the particle in Brownian motion by analysing the frequency content of the signal. This damping is characterized by a relaxation time which is a function of the temperature of the fluid in which the particle is immersed, the viscosity of the fluid, and the inertia of the particle. If the fluid temperature and viscosity are known, the inertia, and thus the size of the particle, may be determined from the relaxation time which is obtained from the Brownian motion detector.

A theoretical analysis of the signal processing strategy was conducted using a Monte Carlo simulation of the particle motion. In the simulation it was possible to determine the relaxation time of the particle from the mean value of the time between the extrema of the signal, which represented the zeros of the Brownian velocity fluctuation. Preliminary analysis of the design of the experiment indicated that the signal to noise of the Brownian detection system was marginal. The performance of the system depended very much on the actual implementation and had to be evaluated experimentally.

A proof-of-concept experiment was conducted using submicron latex spheres of known diameters as test particles. The optics had been designed to approximately the limit of commercially available optical components. The

laser power, however, was not adequate to achieve the required S/N for retrieving the statistical information on the particle Brownian motion. (The argon ion laser, which nominally puts out 2.5 W in a single line, was found to lose 75 percent of its power when operated with a mode selection etalon which was necessary for the present experiment.) The recorded signal was found to be dominated by shot noise. It was estimated that the laser power density needed to be increased by at least a factor of 4 to achieve adequate signal to noise ratio.

While the required laser power density may be easily obtained by using a newer model laser, other physical processes begin to influence the Brownian motion characteristics at high laser beam intensity. An analysis of the effects of thermophoresis and photon pressure was carried out. The effect of thermophoresis due to the uneven heating of the particle by the laser beam was found to be a major limitation so that the application of the method to particles with finite absorptivity (greater than $\sim 10^{-4}$) may lead to erroneous results. The effect of photon pressure was found to be significant for beam intensity greater than 10^{10} W/m^2.

For an experiment to demonstrate the principle, particles of low absorptivity (such as polystyrene) may be used. Our present results suggest that for particles in the 0.1 μm range there would be adequate S/N (~20) if a stable single mode laser with power of 2.5 W is used.

Although the application to soot particles originally envisioned will encounter the limitations on laser beam intensity described above (see Subsection 6.1), other applications may exist, such as refractory oxides in relatively clean combustion systems.

8. ADMINISTRATIVE

8.1 Personnel

The Principal Investigators for this work through almost the entire contract period were Dr. Alan Stanton, a Principal Research Scientist at Aerodyne Research, Inc. and Dr. Wai Cheng, Principal Research Scientist (part-time) at Aerodyne and Associate Professor of Mechanical Engineering, MIT. Dr. Stanton concentrated his research efforts for this program on the development of optical and data acquisition systems for the experimental program, while Dr. Cheng concentrated on the measurement theory, through development of the Monte Carlo Brownian motion simulation model. In addition to his work at Aerodyne on this project, Dr. Cheng supervised the work of two graduate students in the Department of Mechanical Engineering, MIT, Sarah Kostic and Eugenie Hainsworth. This work was in support of the Brownian motion simulation model, funded by a subcontract to MIT.

The laboratory implementation of this program was mostly performed by Mr. Keith McCurdy, who joined the staff of Aerodyne in the second year as a Research Scientist after receiving his Masters degree in Physical Chemistry from Rice University.

In January of 1986 Dr. Stanton left Aerodyne, and his duties as Principal Investigator were assumed by Dr. Joda Wormhoudt. Dr. Cheng continued as Principal Investigator at MIT and supervised the final experimental work.

8.2 Interactions

Three presentations were made at AFOSR Contractors' Meetings on this work during the first year of the contract, one during the second year, and one during the third. These presentations were:

First Year

A.C. Stanton and W.K. Cheng, "Techniques for Submicron Particle Sizing," 1983 AFOSR Contractors Meeting on Air Breathing Combustion Dynamics Research, Scottsdale, AZ, September 19-22, 1983.

W.K. Cheng and A.C. Stanton, "Single Particle Sizing by Measurement of Brownian Motion," 1984 AFOSR Research Meeting on Diagnostics of Reacting Flows, Yale University, March 21-22, 1984.

A.C. Stanton and W.K. Cheng, "Single Particle Sizing by Measurement of Brownian Motion," 1984 AFOSR/ONR Contractors Meeting on Air Breathing Combustion Research, Pittsurgh, PA June 10-21, 1984.

Second Year

W.K. Cheng, A.C. Stanton, and K. McCurdy, "Single Particle Sizing by Measurement of Brownian Motion," 1985 AFOSR/ONR Contractors Meeting on Particle Emission Technology, Monterey, CA, April 16-18, 1985.

Third Year

W.K. Cheng, K. McCurdy, and J. Wormhoudt, "Study of Submicron Particle Size Distributions by Laser Doppler Measurement of Brownian Motion," 1986 AFOSR Contractors Meeting on Diagnostics of Reacting Flows, Stanford, CA, June 16-17, 1986.

8.3 Publications and Patents

No publications or patents resulted from the work reported.

END

5-87

DTIC